ADVANCED MATERIALS
www.advmat.de

Nanoparticle Characterization: What to Measure?

Mario M. Modena, Bastian Rühle, Thomas P. Burg, and Stefan Wuttke**

"Measure that which is measurable and make measurable that which is not"—Galileo Galilei

***What to measure*? is a key question in nanoscience, and it is not straightforward to address as different physicochemical properties define a nanoparticle sample. Most prominent among these properties are size, shape, surface charge, and porosity. Today researchers have an unprecedented variety of measurement techniques at their disposal to assign precise numerical values to those parameters. However, methods based on different physical principles probe different aspects, not only of the particles themselves, but also of their preparation history and their environment at the time of measurement. Understanding these connections can be of great value for interpreting characterization results and ultimately controlling the nanoparticle structure–function relationship. Here, the current techniques that enable the precise measurement of these fundamental nanoparticle properties are presented and their practical advantages and disadvantages are discussed. Some recommendations of how the physicochemical parameters of nanoparticles should be investigated and how to fully characterize these properties in different environments according to the intended nanoparticle use are proposed. The intention is to improve comparability of nanoparticle properties and performance to ensure the successful transfer of scientific knowledge to industrial real-world applications.**

1. Introduction

Nanomaterials are defined as materials that consist of nanoparticles of which at least 50% have one or more external dimensions between 1 and 100 nm.[1] Their small dimensions do not only allow more surface functionality in a given volume, but also lead to physical properties that often differ from their bulk counterparts in many aspects, including electronic, optical, and magnetic features.[2–7] Nanoparticles possess a much higher surface-to-mass ratio than bulk materials and, therefore, surface atoms and surface energy strongly contribute to the material properties, e.g., leading to reduced lattice constants and lower melting points.[8–10] Moreover, the high number of surface atoms and the high surface energy of nanoparticles can have a strong impact on the catalytic performance. Thus, catalytically inactive bulk materials can become very active catalysts when produced as nanoparticles with high surface areas.[11] If fewer atoms comprise a solid, a lower number of orbitals contribute to the band formation. This effect leads to changes in the band structure, such as band gap variations in semiconductors, which depend on the nanomaterial dimensions.[12,13] These unique properties render nanoparticles extremely attractive for a large range of applications, including catalysis, gas and energy storage, photovoltaic, electrical and optical devices, and biological and medical technologies.[14–23] For this reason, nanoparticles are not only a growing topic of interest in research settings, but they are also already widely used in consumer products.[24]

Currently, a key issue hindering the utility of nanoparticles in industry is reproducibility. This problem is, however, partially intrinsic, as the product of synthesis is always prone to yield a polydispersion of nanoparticles, sometimes with a broad distribution of sizes, shapes, and defects. Nanoparticle characterization is therefore a crucial step required to fully comprehend the origin of nanoparticle behavior, and subsequently translate their performance benefits from laboratories into specific real-word applications.

Determining the physicochemical properties of nanoparticles and exploring their structure–function relationships is a critical challenge for scientists today. This endeavor is limited by our ability to fully investigate the nanoscale realm: Different characterization techniques are based on different physical properties, therefore only providing a partial picture of the nanoparticle characteristics. Making matters more challenging

Dr. M. M. Modena
ETH Zurich
Department of Biosystems Science and Engineering
Mattenstrasse 26, 4058 Basel, BS, Switzerland
E-mail: mario.modena@bsse.ethz.ch
Dr. B. Rühle
Federal Institute for Materials Research and Testing (BAM)
Richard-Willstätter - Str 11, 12489 Berlin, Germany
Prof. T. P. Burg
Max Planck Institute for Biophysical Chemistry
Am Fassberg 11, 37077 Göttingen, Germany
Prof. T. P. Burg
Department of Electrical Engineering and Information Technology
Technische Universität Darmstadt
Merckstrasse 25, 64283 Darmstadt, Germany
Prof. S. Wuttke
Department of Chemistry
Center for NanoScience (CeNS)
University of Munich (LMU)
81377 Munich, Germany
E-mail: stefan.wuttke@cup.uni-muenchen.de
Prof. S. Wuttke
BCMaterials
Basque Center for Materials
UPV/EHU Science Park, 48940 Leioa, Spain
The ORCID identification number(s) for the author(s) of this article can be found under https://doi.org/10.1002/adma.201901556.

DOI: 10.1002/adma.201901556

 © 2019 WILEY-VCH Verlag GmbH & Co. KGaA, Weinheim

yet, the characterization methods themselves can directly affect the measured quantities.[2,25–31]

In this critical review we aim at providing a set of guidelines to investigate and characterize the key parameters defining a nanoparticle sample, namely *size*, *shape*, *surface charge*, and *porosity*. We will first define these physicochemical terms and their implication in affecting nanoparticle properties. We will then provide a critical overview of established and specialized techniques currently used for evaluation of nanoparticles, and discuss their practical advantages and disadvantages. Finally, we will propose some reasonable recommendations of how the physicochemical parameters of nanoparticles should be investigated, and how to characterize these key properties in different environments according to the intended nanoparticle use.

Mario M. Modena is a senior postdoc in the group of Prof. Hierlemann, ETH Zurich (Switzerland). He obtained a Ph.D. in physics with Prof. Burg at the Max Planck Institute for Biophysical Chemistry, Goettingen (Germany), where he worked on the development of microfluidic-based and label-free methods for the characterization of biomolecular complexes and nanoparticles in solution. Currently, his research focus is centered on the design of microfluidic platforms for the realization of advanced microphysiological models for application in biology and biomedical engineering.

Stefan Wuttke is leader of the research group "wuttkegroup for science" since 2011, hosted at the Institute of Physical Chemistry at the University of Munich (LMU), at the Center for Nanoscience (CeNS) at the LMU (Germany) and at BCMaterials (Spain). Currently, he is an Ikerbasque Research Professor at the Basque Centre for Materials, Applications and Nanostructures (BCMaterials) in Bilbao. His principal focus is on the design, synthesis, and functionalization of metal-organic frameworks and their nanometric counterparts to target biomedical applications. At the same time, he intends to establish the basic understanding of the chemical and physical elementary processes involved in the synthesis, functionalization, and application of these hybrid materials.

2. Nanoparticle Parameters

Nanoparticles exist in various chemical compositions ranging from micelles to metal(oxide)s, from synthetic polymers to large biomolecules. Each of these materials features a completely different chemistry, which can be analyzed by a variety of methods including optical spectroscopy, X-ray fluorescence and absorbance, Raman spectroscopy, and solid-state NMR.[32] However, often the behavior of nanoparticles is largely governed by their nanometer dimensions. As such, throughout nanoparticle characterization, the investigation of size, shape, surface charge and porosity is a fundamental step for fully understanding and predicting their behavior. These essential parameters are the focus of our review.

The ability to be dispersed into discrete entities, each characterized by a size, shape, surface charge and porosity discriminate nanoparticles from the wider class of nanomaterials encompassing nanostructured objects that might present dimensions in the micro and millimeter regime, such as nanostructured films or nanotubes.[33–35] Size and shape affect the nanoparticle functionalization capacity, fluid drag and diffusion, optical properties, and uptake into cells.[36] Surface charge, besides controlling the stability of a colloidal suspension and its tendency toward aggregation,[37] also plays a major role in shaping the interactions between nanoparticles and the environment.[38,39] Finally, owing to their increased surface-to-volume ratio, nanoparticles possess a large external surface area that can be functionalized for different applications.[17–19] In addition, porous or hollow nanoparticles also exhibit a vast internal surface area, which can be further functionalized to impart additional functionalities, such as the design of smart nanoparticle drug delivery systems.[18,40–44]

In the following, we provide a description of these physicochemical terms in the context of nanoparticle technology, and the different physical and experimental means in which these parameters can be defined.

2.1. Size and Size Distribution

Size refers to the spatial extent of an object. For a spherical object, size can be unambiguously described by one dimension. However, for nonspherical objects, several dimensions are needed to fully define the actual extension of an object in space (**Figure 1**A). While measuring size might appear trivial for objects in the macroscopic scale (>1 mm) where size is measured as the distance between different ends of an object, in the nanoregime size assumes different meanings according to the technique employed to measure it. For a nanoparticle, size can refer to i) its overall physical dimension(s) defined by the atomic structure; ii) an effective size of the particle in a certain matrix according to its diffusion/sedimentation behavior, possibly including adsorption of matrix constituents to the nanoparticle surface, agglomeration or aggregation of the particles in the matrix; iii) an effective size of the nanoparticle, weighted by its mass/electron distribution. This variety of size definitions reflects the wide spectrum of physical approaches that can be used for nanoparticle characterization.

© 2019 WILEY-VCH Verlag GmbH & Co. KGaA, Weinheim

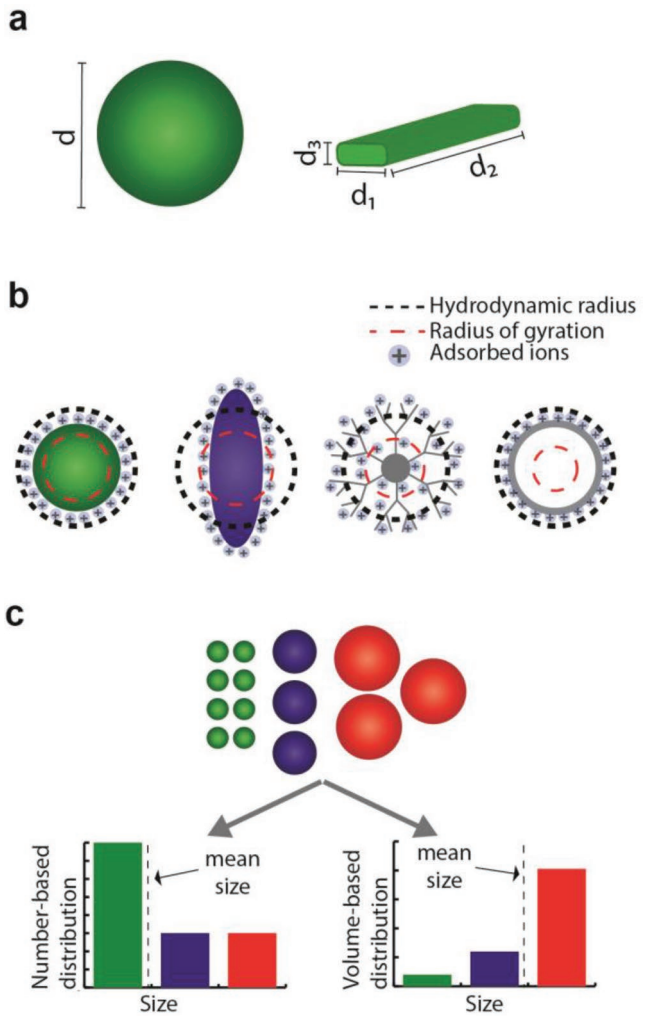

Figure 1. Nanoparticle size characterization. a) Spherical particles are described by a single size parameter. However, for nonspherical nanoparticles, several dimensions are needed to fully report their dimensions; b) the calculation of the effective radius is based on nanoparticle behavior or on the method of detection. The definition of this quantity might differ considerably from the physical nanoparticle dimensions; c) different mean sizes can be calculated for a nanoparticle population according to the weighting factors assigned to the population components.

Nanoparticle size and morphology can be measured at the single-particle level at sub-nanometer resolution using high-resolution microscopy techniques, such as electron microscopy or scanning probe microscopy, providing extremely detailed information on the shape of the nanoparticles under examination. These methods of characterization are based on the interaction between the atomic structure and the impinging electron beam, or with the used scanning probe. However, these techniques usually have limited throughput, are not ensemble techniques (which raises questions such as how representative and statistically relevant the obtained data are), and are carried out under high-vacuum conditions or by placing the sample on a hard substrate, and can therefore neglect important phenomena that may occur in suspension, such as swelling or aggregation. Light-scattering, diffusion- and sedimentation-based methods are commonly employed for the routine analysis of colloidal suspensions. Usually, no direct information on nanoparticle shape can be obtained from these approaches, and an equivalent diameter, corresponding to that of a sphere behaving the same way as the sample under examination (Figure 1B) is usually returned as a characteristic size. To translate this information into actual nanoparticle dimensions, knowledge of nanoparticle shape is required.[29] Finally, static scattering methods, either via light or X-ray illumination, provide information on the mass/electron distribution of the nanoparticles, and hence, indirectly, on the nanoparticle shape.

Although the aim of nanoparticle synthesis is to obtain a monodisperse population of nanoparticles, a real-world sample always displays a certain degree of variation. The nanoparticle size distribution is, therefore, an intrinsic measure of the control and quality of the synthesis procedure, while the estimated size value only refers to an averaged quantity derived from this distribution. Different techniques present different sensitivity to particles of varying dimensions, and care has to be taken when comparing results obtained from different characterization methods.[26,45] Techniques with single-particle resolution, such as high-resolution microscopy and nanoparticle tracking analysis, are able to provide a number-based average of particle size, where each particle is assigned an equal weight. Conversely, scattering intensities scale with particle volume, and size estimation using these methods is based on a volume-weighted (static light scattering) or intensity-weighted (dynamic light scattering) average, which results in a bias toward larger population components (Figure 1C). Although conversions between the types of distributions can be calculated if the weighing factors are known, the conversion might not have a unique solution if the shape of the population distribution is unknown.

Therefore, size estimation is the result of the detection method and of the underlying weighing factors, and of the average quantity that is chosen as representative of a given nanoparticle population. Different averages can be selected, such as arithmetic mean, median value or mode of the distribution. Such a choice should always be stated alongside the reported size estimation. The median, for example, is usually defined as D_{50}, which indicates the nanoparticle diameter at which 50% of the population lies below. One single quantity, however, is not sufficient to describe a whole population because similar average values might correspond to largely different distributions. To provide more information, different metrics are commonly used, with the most common ones being the D_{10} and D_{90}, corresponding to the value of diameter which encompasses 10% and 90% of the population, respectively, or the standard deviation, when the population follows a normal distribution. Derived quantities can then be calculated from these metrics, such as the coefficient of variation (COV), defined as the ratio of standard deviation and arithmetic mean, used for static light scattering measurements and defined by the ISO 13320 standard.[46]

2.2. Shape

Although often assumed spherical, nanoparticles feature a large variety of geometric and irregular shapes.[47] Particles

© 2019 WILEY-VCH Verlag GmbH & Co. KGaA, Weinheim

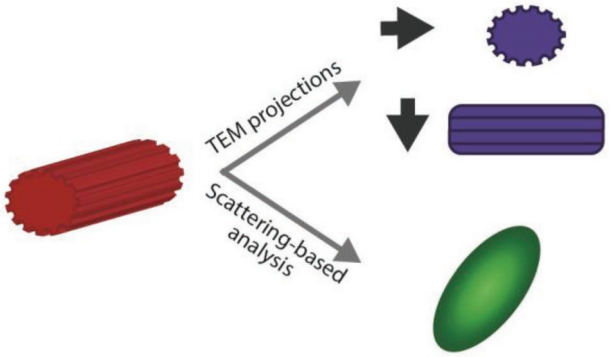

Figure 2. Nanoparticle shape characterization. TEM provides nanometer resolution on nanoparticle morphology. However, the measured shape is a 2D projection of the nanoparticle morphology, and therefore depends on the relative orientation of the nanoparticle and the electron beam. Scattering-based techniques provide qualitative information on the nanoparticle shape.

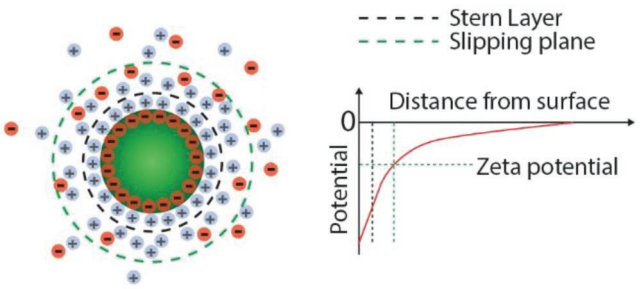

Figure 3. Surface charge and zeta potential of nanoparticles in suspension. Charges on the nanoparticle surface are screened by the free ions in solution, giving rise to two ion layers: a first layer of adsorbed ions on the nanoparticle surface, the so-called Stern layer; a second layer of stationary but diffusing ions that move with the particle. The zeta potential is defined as the potential difference between the slipping plane, i.e., the plane that "separates" the cloud of stationary ions around the particles from freely diffusing ions in solution, and the potential of the bulk solution.

with equal composition and similar dimensions might present drastically different behaviors as a consequence of their shape, such as surface-binding capability, cellular uptake and release, optical and plasmonic effects,[47–51] to name some of the major properties affected by particle morphology.

Shape is commonly characterized by use of high-resolution microscopy techniques, such as electron and scanning probe microscopy, which enable the detection of particle morphology with sub-nanometer resolution. These techniques are routinely employed during nanoparticle synthesis for validation and characterization of synthesis outcome. However, electron microscopy typically provides a 2D projection of the particle shape onto a plane, which, for specific cases of highly anisotropic particles, might lead to erroneous estimates of the particle morphology (**Figure 2**). To circumvent this limitation, the characterization of particles presenting distinct 3D anisotropy can be carried out by acquiring the projections of a large number of randomly oriented identical particles to reconstruct their spatial arrangement,[52] or by electron tomography.[52,53]

Information on shape and anisotropy of particles in solution can also be obtained by using scattering-based techniques, which can more readily be applied in solution, such as by combining static and dynamic light scattering characterization.[54] However, the underlying ensemble-based analysis of the particles in solution only enable to infer, quantitatively, an anisotropy factor of the particles, and a detailed study of particle morphology remains limited to high-resolution microscopy. Nevertheless, the qualitative shape information obtained by scattering-based characterization methods are often necessary to confirm microscopy results, as sample preparation and electron-microscopy evaluation might affect the sample agglomeration state or induce damages to the particle framework.

2.3. Surface Charge

The boundary between the solid and the fluid phase is a dynamic environment, and multiple phenomena, such as the presence of dangling bonds, or the adsorption or grafting of charged molecules contribute to the appearance of a net charge on the nanoparticle surface. This charge has a primary effect on the behavior of nanoparticles in different environments, in particular on controlling their tendency toward aggregation, as electrostatic repulsion between particles is a key factor promoting the stability of colloidal solutions.[55] In particular, in an electrolyte solution, mobile charges in solution are attracted by the static charges on the nanoparticle surface, effectively leading to a screening of the electric potential, which can ultimately result in particle aggregation. A typical measure of surface charge and colloidal stability is given by the zeta potential ζ, which is defined as the electric-potential difference between the stationary layer of charges surrounding the particles and the solution potential (**Figure 3**).[56] Suspensions that feature $|\zeta| \geq 15$ mV are usually considered to be colloidally stable. Several parameters affect the zeta potential of particles in solution, namely the ionic strength of the solvent, the presence of charged or uncharged molecules that can adsorb on the particle surface, and the pH of the solution. In particular, when dealing with particles that have (de)protonatable groups on their surface, one parameter of interest is represented by the pH at the point of zero charge, pH_{pzc}, i.e., the pH value at which the particles present zero charge on their surface,[57] and hence show a major tendency toward forming large aggregates.

Finally, surface charge also has major implications on controlling the interactions between nanoparticles and biological fluids and samples. The formation of a protein corona on the surface of the nanoparticles and the probability of nanoparticle uptake by different types of human cells and tissues largely depend on the nanoparticle surface charge.[38,58] For these reasons, the investigation of surface charge is a fundamental step in the formulation of nanoparticle-based therapeutics.[59]

2.4. Porosity

The possibility of synthesizing nanoparticles featuring porous frameworks has greatly expanded the range of application of nanomaterials.[60,61] Porosity provides the nanoparticles with a drastic increase in their surface-to-volume ratio, which can

© 2019 WILEY-VCH Verlag GmbH & Co. KGaA, Weinheim

exceed that of solid particles with equal dimensions by several orders of magnitude. Over the last two decades, porous nanoparticles have attracted considerable attention in the pharmaceutical and medical fields for delivery and targeting of therapeutics[62–65] and for disease diagnostics.[21,66] These functionalized nanoparticles have to fulfill diverse tasks during the delivery process, e.g., drug loading, nanoparticle sealing, targeting and cell uptake, endosomal escape, and controlled and triggered release of the drug.[20] For enabling such a wide spectrum of functions, a chemistry has to be developed for the integration of sophisticated inner and outer surface functionalizations:[18] inner pore functionalization for controlled host-guest interactions,[67] and peripheral (outer) functionalization for targeting purposes and drug release at the intended target site.[43,68] The "orthogonality" of the inner and outer surface chemistry is key in providing such capability to nanocarriers, as it allows to differentiate between the targeting moieties or gatekeepers grafted on the nanoparticle surface and the functional groups attached to the inner surface. Besides "orthogonal" functional groups or derivatization reactions, steric hindrance or electrostatic repulsion can also be used to control the site selectivity of the functionalization and the type of molecules that can enter the pores, and hence provide controlled reaction environments.

To enable the development and characterization of porous nanoparticles, porosity needs to be investigated at different levels (**Figure 4**), namely, i) the size of the pore opening; ii) the dimensions and volume of the porous cavity; iii) the interconnection of the porous structure, i.e., whether only superficial pores are accessible from the outside or the whole internal porous network; iv) specific surface area (sum of inner and external surface); v) surface-to-volume ratio; vi) the inner and outer surface functionalization. Despite the large interest in this class of nanomaterials, there is a general lack of standardized methods to investigate at depth all these key features of porous nanoparticles. In the case of a crystalline material, the periodic arrangement of individual building blocks of a nanomaterial in the crystal lattice can give rise to porosity, and when the crystal structure is known, the pore sizes and pore openings can be calculated. Moreover, the porosity of crystalline and noncrystalline nanomaterials can also be measured with different techniques such as gas sorption. Although these approaches can provide fundamental insights into the pore structure of dry particles, they fail to predict possible variations that could occur in solution, such as selective permeation of solvent components within the porous framework. In our discussion, we will also present some specialized techniques that can overcome such limitations in characterization and offer new information on porous nanoparticles in solution.

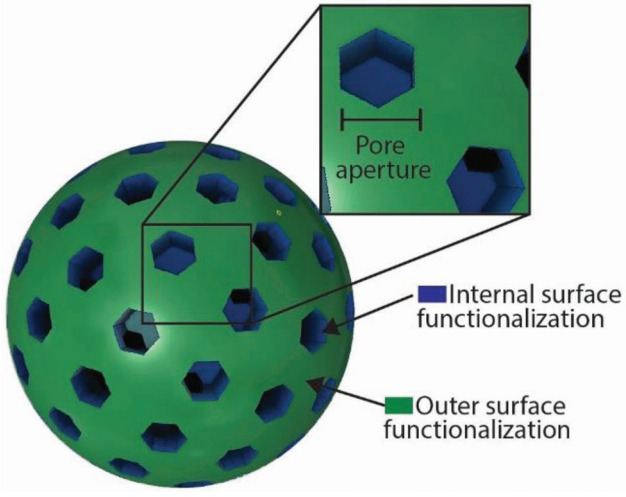

Figure 4. Porous nanoparticle. Porous nanoparticles feature different characteristics of interest which need to be characterized, namely, pore aperture, pore volume, and external and internal surface functionalization.

3. Characterization Methods

Several characterization methods have been devised to investigate size, distribution, shape, surface charge and porosity of nanoparticles in different environments. Here, we discuss the main techniques for the characterization of these key parameters both in the dry state and in solution. We also introduce some specialized techniques for nanoparticle characterization, which enable to expand the accessible range of information to gain deeper insights into specific nanoparticle properties. Given the large number of existing approaches and techniques, including the combination of different methods in "hyphenated" techniques, different variations of the same techniques, and different approaches to data analysis for a same technique, this article cannot provide an exhaustive list of all available methods for nanoparticle characterization. We rather provide a selection of methods that in our opinion are best suited to characterize a broad range of nanomaterials, which are commonly used and well established.

3.1. Characterization in Dry State

The methods discussed in this section are summarized in **Table 1**.

3.1.1. Transmission Electron Microscopy (TEM)

Transmission electron microscopy is undoubtedly one of the most important nanoparticle characterization techniques. TEM employs a focused electron beam on a thin (typically less than 200 nm) sample to produce micrographs of nanoscale materials with high lateral spatial resolution[69,70] (**Figure 5**a). Current electron microscopes can achieve resolutions down to 0.05–0.1 nm by reducing image distortion by aberration correctors, hence providing high-resolution images with atomic resolution.[71,72] TEM also enables studying the crystalline structure of selected microscopic regions of crystalline materials by spatially confining and focusing the impinging beam and detecting the resulting electron diffraction pattern.[73] Thanks to this high spatial resolution and selectivity, TEM enables the investigation of size, shape, and crystal structure at the single-particle level. Once a representative group of images of the nanoparticle sample is acquired, the individual size of ≈1000 randomly

© 2019 WILEY-VCH Verlag GmbH & Co. KGaA, Weinheim

Table 1. Summary of characterization methods for dry nanoparticles.

Technique	NP[a)] state	Parameters	Advantages	Limitations	Reviews
TEM	High vacuum	*Size* (<1 nm to <1 µm) *Size distribution* (number-based) *Shape* (2D projection)	Particle morphology at sub-nm resolution, information on internal structure of the particles	High energy beams, very expensive	[78,80]
SEM	High vacuum or low pressure	*Size* (≈2–3 nm to >10 µm) *Size distribution* (number-based) *Shape* (2D projection)	Single-particle resolution, lower energy beams than TEM, user friendly	Limited penetration depth	[84,87,88]
AFM	Dry and in liquid	*Size* (≈10–20 nm lateral res., <1 nm vertical res.) *Size distribution* (number-based), *Shape* (3D imaging)	High compatibility with different samples and measurement environments	Samples need to be deposited on hard surface, limited throughput	[89]
XRD	Dry	*Crystallite size* (≈1 to ≈100 nm)	Rapid, provides information on crystal structure	No information on particle size	[99,100]
SAXS	Dry and in suspension	*Size: radius of gyration* (≈1 nm to ≈1 µm) *Size distribution* (intensity-based) *Shape* (through modeling)	High sensitivity, compatible for both dry particles and in suspension	Previous knowledge of particle morphology is required for fitting the data	[102]
MS	Dry and in suspension	*Size* (≈0.1 to ≈50 nm) *Size distribution* (number-based) *Composition*	Information on elemental composition	Sample ionization (might affect particle stability)	[105,106]
Gas sorption	Dry	*Surface area* *Pore volume* *Pore size distribution* (≈1 to ≈50 nm)	Compatible with polydisperse and aggregated samples	Requires sample degassing, no information on particle morphology	[121,122]

[a)]NP stands for nanoparticle.

selected nanoparticles should be measured to obtain meaningful statistics for size distribution determination. This procedure can be done either manually (inherently affected by human errors, bias, and subjectivity) or using automated particle analysis methods.[74–77]

Although TEM enables visual inspection of single particles with nanometer resolution, the whole workflow of sample preparation, measurement, and analysis can be extremely labor intensive.[78,79] In addition, the nanoparticles have to be electron transparent and able to withstand the high vacuum and beam energy employed during characterization. Especially, due to the high-energy electron beam, sample damage is a known problem for organic, polymer and hybrid nanoparticles[26,80,81] (Figure 5). This challenge can be addressed by using Cryo-EM (see advanced methods) or by reducing the acceleration voltage, however at the expense of increasing the complexity of the measurement procedure or reducing the attainable resolution.[80,82] Lastly, TEM is a highly costly technique (acquisition and maintenance costs), and requires highly trained personnel.

3.1.2. Scanning Electron Microscopy (SEM)

Scanning electron microscope enables imaging the sample surface by detecting secondary electrons emitted from the sample upon interaction with the impinging electron beam[83] (**Figure 6**a). In SEM, lower beam energies are utilized for sample imaging as compared to TEM characterization, which results in a limited penetration depth of the beam and, hence, in being sensitive solely to the specimen surface. However, this superficial interaction also implies that SEM characterization can be used for the analysis of the morphology of "thick" (>100 nm) samples, which is not possible with TEM.[84–86] The moderate electron energies employed for SEM analysis limit the resolution to typically >2–3 nm, however at the same time drastically decrease the possibility of beam-induced sample damage compared to TEM. In addition, SEM is by far more user-friendly and enables faster measurements, and features lower acquisition and maintenance costs than TEM. SEM instruments typically also enable investigating the composition

© 2019 WILEY-VCH Verlag GmbH & Co. KGaA, Weinheim

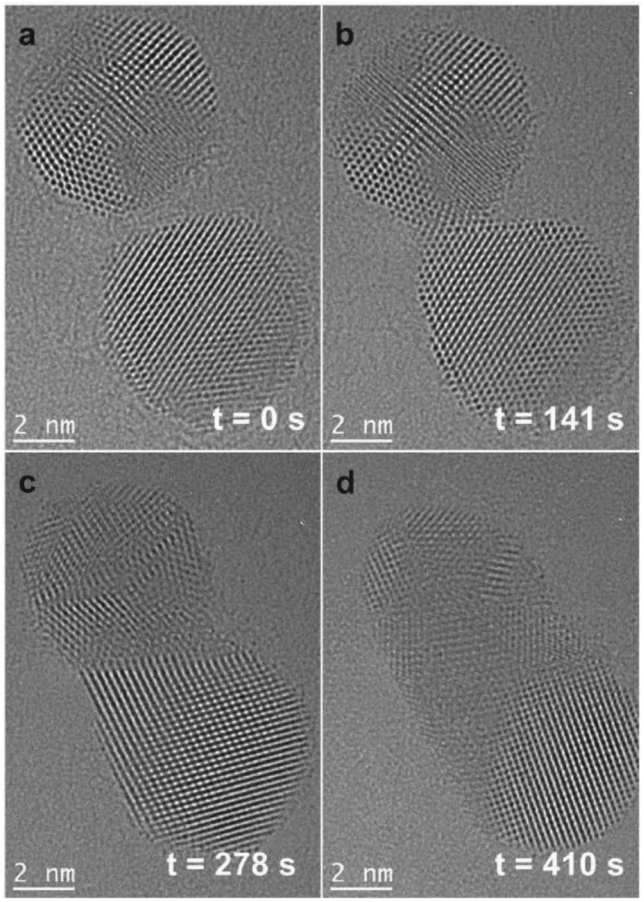

Figure 5. Electron beam–induced sample modifications observed in TEM. The temporal sequence of high-resolution TEM images shows the coalescence of two gold nanoparticles caused by the electron beam during long-term acquisition. Reproduced with permission.[70] Copyright 2012, American Chemical Society.

of the sample surface by measuring the amount of elastically backscattered electrons, which depends on the interaction between the focused electrons and the sample material, or by detecting x-ray emission due to e-beam ionization.[84,85]

SEM typically requires conductive substrates for high-resolution imaging and nonconductive samples can be coated with a thin (5–10 nanometer) metallic film before being analyzed. This modification of size and surface structure of nonconductive nanoparticles due to sample preparation has to be accounted for when interpreting SEM micrographs. Environmental SEM, i.e., SEM imaging performed at low pressure instead of high vacuum, enables imaging nonconductive samples, as surface ionization can be reduced by interaction with the low-pressure gas in the measurement chamber.[87,88] However, this method of detection delivers lower spatial resolution than standard SEM imaging. Finally, when comparing SEM and TEM images, it should be kept in mind that SEM only yields information on the sample surface structure, while TEM interacts with the whole sample volume, hence providing information on sample structure (e.g., it can provide information on the layer thicknesses of core/shell nanoparticles) (Figure 6b,c).

3.1.3. Atomic Force Microscopy (AFM)

Atomic force microscopy is a scanning probe microscopy technique that can be used to probe and visualize the surface (and several other force-related quantities) of nanometer-sized or even atomic-sized objects.[89–92] A sharp tip at the end of a cantilever is rastered across the surface of a sample, and the forces the cantilever experiences during the measurement as a result of the interaction of the tip with the sample are recorded with the help of a laser beam reflected off the tip of the cantilever onto a photodiode array. Depending on the measurement mode, this can either be a vertical or lateral deflection of the cantilever, or a change in amplitude, frequency, or phase of an oscillating cantilever. In general, three different modes are used: contact mode, noncontact mode, and tapping mode. In contact mode, the tip is always in direct contact with the surface of the sample. The repulsion of the tip and the surface atoms of the sample result in a vertical deflection of the cantilever, depending on the underlying topography. The lateral deflection of the cantilever can be used in lateral force microscopy (LFM) and measures changes in friction which often occur at the boundary of two different materials. This mode is generally quite robust, but it

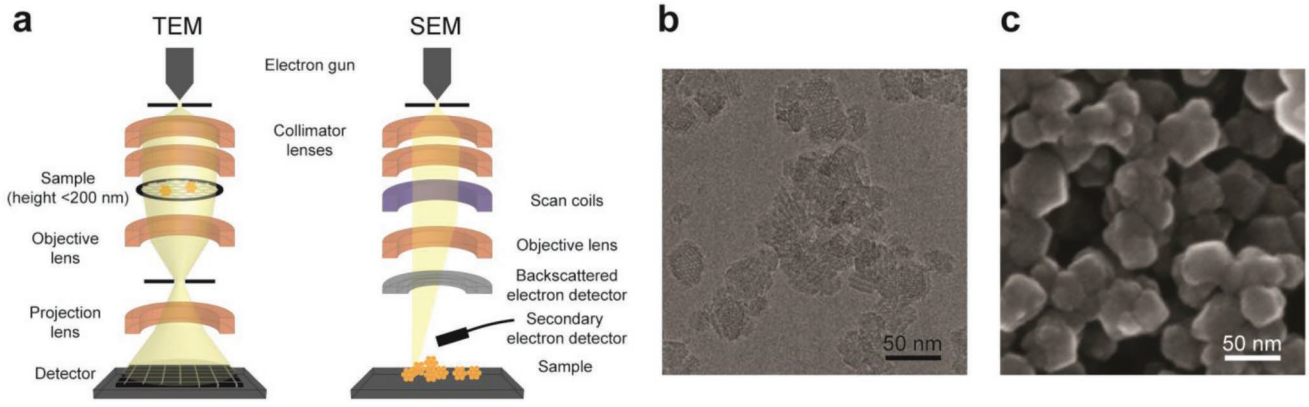

Figure 6. TEM versus SEM. a) Simplified schematic of TEM and SEM instruments; b) TEM micrograph of MIL-101(Cr). The crystalline structure of the particles is clearly visible; c) SEM micrographs of the same particles as in (b), after coating with a thin layer of carbon to avoid sample ionization. b,c) Reproduced under the terms of the Creative Commons Attribution-NonCommercial license.[217] Copyright 2018, The Authors. Published by Wiley-VCH.

© 2019 WILEY-VCH Verlag GmbH & Co. KGaA, Weinheim

is not noninvasive and can result in a displacement of nano-objects on a surface, and wear or even damage of the sample or the tip. In noncontact mode, a piezocrystal is used to drive oscillations of the cantilever at or close to its resonance frequency. These oscillations occur slightly above the surface of the sample, and the tip is never in direct contact with the sample surface. Yet, a change in the force between the tip and the sample surface results in a shift of the amplitude, resonance frequency, and phase of the cantilever oscillations, which can be used to draw conclusions about surface properties such as surface topography. This mode is usually used in (ultra) high vacuum, and can achieve very high resolutions, down to the atomic level.[93] Tapping mode (or intermittent contact mode) is similar to noncontact mode. An oscillating cantilever is used as well, but instead of oscillating strictly above the sample surface, the tip "taps" on the surface during the oscillations. This mode is much less invasive than contact mode and is most commonly used under atmospheric conditions. It can even be used in liquids. Besides the attractive or repulsive forces between the tip and the atoms on the sample surface that change depending on the distance between the cantilever and the surface atoms (and hence with surface topography), various other parameters can be investigated with AFM, such as magnetic forces in MFM, chemical forces in CFM, or the surface potential in KPM. If the nano-objects are directly on the surface of an (ideally smooth and flat) substrate, no specific sample preparation is necessary prior to the measurement. Particles in suspension have to be deposited on a smooth surface (such as mica or a silicon wafer) first. Unlike in scanning tunneling microscopy, electric conductivity is not necessary for a standard topography scan in AFM. The scanned image shows directly the size and morphology of the nano-objects. However, it is worth noting that the size in the *z*-direction is usually very precise, while the lateral size (and shape) is a convolution of the nano-objects and the size/shape of the probe tip. Typically, the scanned area is limited to tens or a few hundreds of micrometers, and depending on the measurement mode and the size of the scan area, image acquisition can take several minutes.

3.1.4. X-Ray Diffraction (XRD)

X-Ray diffraction is a versatile technique used to investigate a wide range of structural aspects in crystalline samples. The attainable information ranges from microscopic features, such as the arrangement of the crystal components, to macroscopic information, such as the mean shape and size of crystals. This information can be obtained by analyzing the full width at half-maximum (FWHM) of the Bragg reflections. Since every Bragg peak is associated with a unique crystallographic direction, the FWHM is influenced by the number of atoms contributing to the scattering events and this number is directly connected to the size of the crystal planes generating the specific reflection. Different sizes for different crystallographic directions are associated to a specific shape (i.e., morphology) of the crystallites, which can therefore be refined against the XRD pattern.

For a defined crystallographic direction, the mean value of the crystal size can be estimated by using the Scherrer equation (Equation (1)), often erroneously referred to as Debye–Scherrer equation.[94] This equation considers the ideal condition of a perfectly parallel, infinitely narrow and monochromatic X-ray beam incident on a monodisperse powder of cube-shaped crystallites.[95] The equation is

$$D_{hkl} = \frac{K\lambda}{B_{hkl}\cos\theta} \tag{1}$$

where D_{hkl} is the crystallite size in the direction perpendicular to the lattice planes, *hkl* are the Miller indices of the planes belonging to the peak that is being analyzed, K is a numerical factor commonly referred to as the crystallite-shape factor,[96] λ is the wavelength of the X-rays, B_{hkl} is the FWHM of the diffraction peak in radians, and θ is the Bragg angle. Given the strong assumptions regarding the instrumental ideality, the extracted mean size value always needs to be corrected for instrumental broadening effects. Standard phases with known crystal size and narrow size distribution are commonly used to calculate the instrumental broadening, or $\mathrm{FWHM}_{\mathrm{instr}}$, whose contribution needs to be subtracted from the FWHM used in the Scherrer equation.

Although this equation constitutes a valuable approach to estimating the mean crystallite size of a polycrystalline sample, the user must be aware of some important issues. First, when reflections related to different crystallographic directions are used for extracting a unique value of crystallite size, any information regarding the crystal shape is lost as the final size value is averaged over all the crystallographic directions. Second, other structural features of the sample contribute to the peak broadening besides crystal size, such as lattice strain, defects or the nanoparticle size itself,[97–100] resulting in overestimated FWHM values and consequent underestimated crystal size. Lastly, but most importantly, the information available by XRD experiments arises from the structural properties of crystal domains and not necessarily from the entire particle.[101] For this reason, when analyzing particle sizes, the use of different analysis methods, such as TEM or SEM, is necessary to obtain reliable information.

3.1.5. Small-Angle X-Ray Scattering (SAXS)

Small-angle X-ray scattering is a very versatile method for the characterization of nanomaterials.[102–104] The sample is illuminated with X-rays and the scattered irradiation is registered by a detector at small angles, usually between 0.1° and 5°. Based on the intensity distribution of the scattered X-ray photons that are passing through the sample, information about particle size, size distribution, morphology, crystallinity, molecular weight, and agglomeration can be obtained. If the absolute intensity that is monitored by the detector is properly calibrated, information about particle concentration or porosity is also available. The samples can be solids, powders, composites, or dispersions of nanoparticles in a liquid medium. Being an ensemble method, SAXS probes a very large number of nano-objects simultaneously, and the measured data gives a statistically relevant average over a large portion of the sample. Moreover, only minimal sample preparation is required, the measurement is usually nondestructive, and can often be used under in situ

© 2019 WILEY-VCH Verlag GmbH & Co. KGaA, Weinheim

or in operando conditions to study colloidal nanosystems in their native state. The recorded SAXS pattern consists of two components, namely the form factor, which contains information about mean structural properties of the nanoparticle (i.e., morphology and size), and the structure factor, which can yield information about the positional correlation of the nanoparticles (e.g., if the particles interact with each other and assemble into higher order structures). However, for nonidentical and nonspherical particles, approximations such as the decoupling approximation (assuming that particle size and shape are independent of their spatial position) or the local monodisperse approximation (assuming that at short ranges all particles are identical) have to be used in order to separate the recorded intensity values into a product of form factor and structure factor. Also, due to the polydispersity and nonuniformity of any synthesized nanomaterial, some prior knowledge of the sample is often required to impose certain constraints on the model used to describe the data, since the solution might be ambiguous if all possible sizes and shapes are allowed.[102]

3.1.6. Mass Spectrometry (MS)

Mass spectrometry was used originally for the characterization of nanoparticle composition by revealing the stoichiometry of their building blocks after digestion and dissolution. With the introduction of soft ionization techniques, such as electrospray ionization (ESI) and matrix-assisted laser desorption ionization (MALDI), and methods of separation and detection able to analyze samples in the Megadalton range, such as ion-mobility spectrometry (IMS), time-of-flight (TOF) analysis, and single-particle inductively coupled plasma-mass spectrometry (single-particle ICP-MS), the range of application of MS has been extended to the analysis of intact nanoparticles ranging from few nanometers to hundreds of nanometers in diameter.[105–108] Thanks to the versatility of the analysis methods, MS has been used to investigate a variety of nanoparticle properties besides elemental composition.[107–109] Integration of nanoparticle size separation and MS detectors made it possible to study the number concentration and size distribution of nanoparticles of a few tens of nanometers with single particle detection capability.[110–113] MS is also unique in providing information on the functionalization layer grafted on the surface of nanoparticles.[114,115] Furthermore, MS has often been applied in the investigation of interactions between nanoparticles and biomolecules after exposure to biological fluids to identify and quantify the composition of complex protein coronas on the nanoparticle surface.[116–118] Finally, the ability of MS to ionize and investigate soft materials, such as tissues, has rendered this technique invaluable in studying the biodistribution and uptake of nanoparticles within different organs upon administration of nanoparticle solutions for toxicology studies.[119,120]

3.1.7. Gas Sorption

Analyzing the adsorption and desorption of gas molecules (e.g., nitrogen) under isothermal conditions on solid surfaces is a widespread technique for the characterization of porous bodies. By recording the adsorption and desorption isotherms, fundamental data including the surface area, pore size distribution and accessible pore volume of a given material can be obtained.[121,122] These different properties are determined by the evaluation of sorption isotherms using different data analysis techniques such as the Brunauer–Emmett–Teller (BET) method. Sorption isotherms are subdivided into eight different types according to the IUPAC definition.[123] The experimental data allow the classification of the investigated material as microporous (pore size below 2 nm), mesoporous (between 2 and 50 nm), or macroporous (above 50 nm).

For nonporous materials, the volume-specific surface area (VSSA) can be used to classify it as a nanomaterial.[124–127] VSSA is defined according to Equation (2)

$$\mathrm{VSSA} = \frac{S}{V} = \mathrm{SSA} \times \rho \tag{2}$$

where S is the external surface of the sample, V is the solid volume, SSA is the specific surface area (surface per mass), and ρ is the material density. According to the European Commission (EC) recommendation, a material with a VSSA larger than 60 m^2 cm^{-3} can be considered a nanomaterial.[128,129] The external surface can be readily measured for nonporous nanomaterials via gas adsorption measurements and by analyzing the results with the BET method. However, for porous nanoparticles the BET surface area is a sum of the external and internal surface. This implies that the external surface has to be extracted by using a modified *t*-plot approach.[125] The basic principle of this method is to compare the measured gas adsorption isotherm with a reduced form of standard isotherms (the *t*-curves) measured for nonporous solids. For this comparison, the adsorbed nitrogen volume is plotted against the thickness t of the adsorbed layer as obtained from the standard isotherms for the material in question (e.g., silica, alumina, carbon). In an intermediate partial pressure range (p/p_0 = 0.25–0.55), this comparison usually results in a linear relationship with the slope relating to the BET value. If a second linear part can be observed at higher partial pressure values ($p/p_0 > 0.6$), the slope of this second part can be related to the external surface. Likewise, if a linear relationship is also measured at lower partial pressure range ($p/p_0 < 0.3$), the slope can be used to extract the internal surface area.

3.2. Characterization in Suspension

The methods discussed in this section are summarized in **Table 2**.

3.2.1. Dynamic Light Scattering (DLS)

Dynamic light scattering estimates the particle size from the Brownian diffusion of the particles in solution. The low sample amount required for analysis, the short acquisition and analysis times (in the range of few minutes in total per sample), the dynamic range spanning from nanometer to ≈10 µm, and the compatibility of the technique with a large variety of solvent

© 2019 WILEY-VCH Verlag GmbH & Co. KGaA, Weinheim

Table 2. Summary of characterization methods for nanoparticles in suspension.

Technique	NP[a)] state	Parameters	Advantages	Limitations	Reviews
DLS	In suspension	*Size: hydrodynamic radius* (≈5 nm to ≈10 µm) *Size distribution* (intensity-based)	Rapid, provides information on nanoparticle behavior in solution	Highly biased toward larger particles in suspension, no information on particle shape	[134]
SLS	In suspension	*Size: radius of gyration* (≈5 nm to ≈1 µm) *Size distribution* (intensity-based)	Molecular weight and radius of gyration of particles in solution	Highly biased toward larger particles in suspension	[29,136]
NTA	In suspension	*Size: hydrodynamic radius* (≈30 nm to ≈1 µm) *Size distribution* (number-based) *Concentration*	Single-particle resolution, suitable for highly polydisperse samples	Requires sample dilution and highly scattering particles	[138]
Electrophoretic light scattering	In suspension	*Zeta potential*	Rapid, typically combined with DLS	Indirect estimation of zeta potential from electrophoretic mobility, ensemble-based	[139]
AUC	In suspension	*Size: hydrodynamic radius* (≈1 nm to <1 µm) *Distribution* (population-based) *Mass* and *density*	High-sensitivity, compatible with multimodal population	High-cost equipment Highly trained users	[143]
SEC	In suspension, porous structure	*Size* (≈1 to ≈200 nm) *Size distribution* (population-based)	Provides highly monodisperse sample fractions, compatible with industrial settings	Absolute size quantification might be challenging due to particle-solid phase interaction	[147]
FFF	In suspension	*Size* (≈1 nm to ≈50 µm) *Size distribution* (population-based)	Highly tunable (different accumulation forces can be used) Provides monodisperse sample fractions	Sample recovery and choice of experimental parameters can be challenging	[155,156]
FCS/FCCS	In suspension	*Size* (≈1 nm to ≈1 µm) *Size distribution* (according to fluorescence labeling)	Selectivity provided by the fluorescence detection	Need of fluorescent labels (if sample is not fluorescent)	[159]
TRPS	In suspension (conductive solution)	*Size* (≈50 nm to 10 µm) *Size distribution* (number-based) *Shape* *Concentration* *Zeta potential*	Tunable detection range, single-particle resolution, provides information on surface charge	Requires (highly) conductive solutions, requires careful calibration	[163,164]

[a)]NP stands for nanoparticle.

compositions render DLS extremely suitable for routine and rapid characterization measurements.

DLS size estimation is based on the determination of the free diffusion coefficient of suspended particles.[130] A laser is transmitted through a measurement cell containing the particle suspension, and the random thermal motion of the particles causes time-dependent fluctuations of the intensity of the scattered light (**Figure 7**a). The time correlation of these fluctuations is directly dependent on the diffusion time of the scattering objects, i.e., the particles, through the laser spot. An autocorrelation analysis of the time-domain signal is then used to estimate the diffusion coefficients of the particles, which are proportional to the scattering correlation time, and to investigate the population size distribution, which affects the shape of the autocorrelation curve.

Particle size is then inferred from the diffusion coefficient through the Stokes–Einstein equation (Equation (3))[130]

$$D = \frac{k_B T}{6\pi\eta R_h} \tag{3}$$

where D is the diffusion coefficient, k_B is the Boltzmann constant, T indicates the temperature at which the analysis is carried out, and η is the kinematic viscosity of the solvent. R_h indicates the hydrodynamic radius of the particles, i.e., the radius of a spherical particle whose diffusivity equals that of the sample under examination. For nonspherical particles, R_h can differ significantly from the actual particle dimensions, and previous knowledge of particle shape is required to translate this parameter into more representative size estimates.

DLS is an ensemble-based technique, and care needs to be taken when interpreting measurements of particle suspensions with a high level of polydispersity (Figure 7b,c). Different algorithms have been developed to interpret the correlation function resulting from polydisperse populations of particles.[131–133]

© 2019 WILEY-VCH Verlag GmbH & Co. KGaA, Weinheim

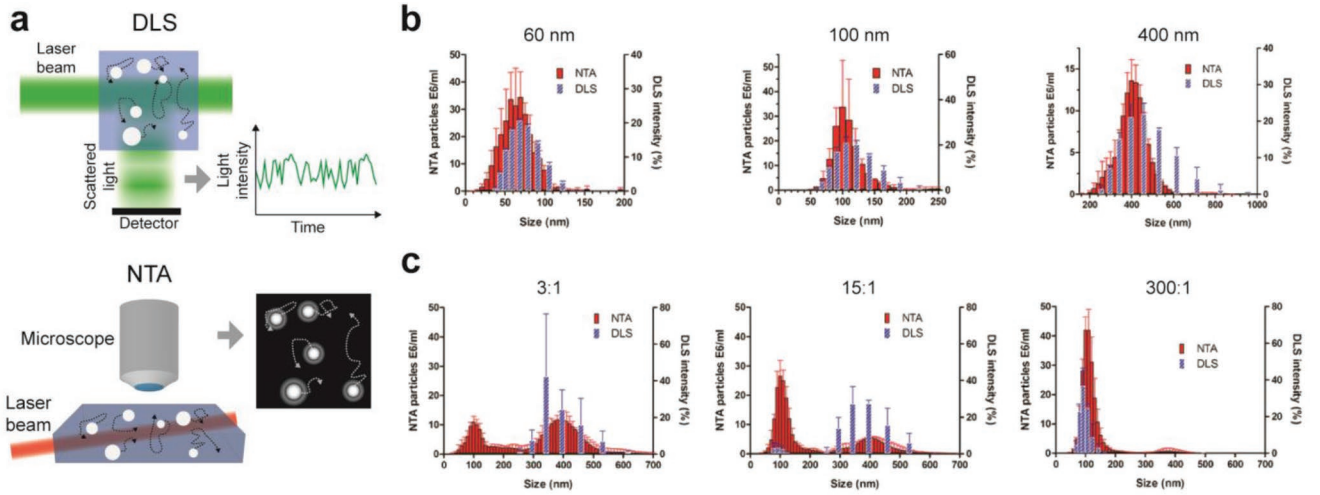

Figure 7. DLS and NTA. a) Schematic illustration of DLS (top) and NTA (bottom) instruments. DLS measures the scattered-light fluctuations caused by the Brownian motion of particles in solution. NTA tracks particle diffusion by video acquisition; b) comparison of size characterization of monodisperse nanoparticle samples by DLS and NTA; c) comparison of size characterization of bimodal dispersions of polystyrene nanoparticles of 100 and 400 nm nominal size. The ratios on the top of the graphs indicate the concentration ratio of the 100 and 400 nm particles in solution. (b,c) Adapted with permission.[138] Copyright 2010, The Authors. Published by Springer Nature.

However, due to the high dependence of scattering intensity on particle size, size estimation is typically biased toward the larger population components.[134] Therefore, sample-size fractionation prior to data acquisition is the most effective route to ensure correct estimation of size parameters for highly polydisperse sample populations.[135]

Finally, DLS can be carried out on any optically clear particle suspension, provided that the kinematic viscosity of the solvent is known or is characterized by using calibrated monodisperse particle suspensions.

3.2.2. Static Light Scattering (SLS)

Static light scattering is used to estimate the radius of gyration and the molecular weight of proteins and nanoparticles in suspensions. The radius of gyration r_g (Equation (4)) represents the mass-weighted radius of the particle and it is defined as

$$\left\langle r_g^2 \right\rangle = \frac{\sum_i m_i r_i^2}{m_i} \tag{4}$$

where m_i and r_i are the mass and distance from the center of mass, respectively, of the ith element composing the particle.[29] As an example, $r_g = \sqrt{\frac{3}{5}a^2}$ for a spherical particle, where a is the particle radius. As such, a priori knowledge of particle shape is necessary to properly relate the estimated radius of gyration to the particle dimensions.[29]

Molecular weight and radius of gyration are estimated by measuring the time-averaged intensity of light scattered by a colloidal suspension at different concentrations.[54] A Debye plot is then generated by plotting the variation of scattering intensity as a function of particle concentration, and the slope and intercept at zero concentration of the obtained curve can then be used to calculate the molecular weight and the radius of gyration of the particles in solution.[54,136] This relation is theoretically valid only for zero-angle scattering. However, the scattering intensity cannot be measured at this angle due to the transmitted light. For particle below ≈40 nm, scattering can be measured at a single angle and used to estimate the zero-angle scattering intensity.[29] In contrast, for larger particles, the measurement at multiple scattering angles is necessary due to the different forward and backward scattering intensities. SLS is an ensemble-based measurement technique and, as for DLS, scattering intensity scales dramatically with particle size. For polydisperse particle populations, the use of sample fractionation is advisable to properly estimate the radius and molecular weight of the particles in suspension.[29]

3.2.3. Nanoparticle Tracking Analysis (NTA)

Similar to DLS, nanoparticle tracking analysis provides size characterization based on the free diffusion behavior of particles in solution. NTA measures particle diffusion by tracking the random motion of single particles in solution via high temporal-resolution video acquisition and enhanced contrast microscopy[137] (Figure 7A). NTA measures the diffusion of the objects in suspension with single-particle resolution, and hence it is particularly suitable for the characterization of size distribution for highly polydisperse nanoparticle populations (Figure 7b,c). NTA can be used for measuring particles with hydrodynamic radii ranging from ≈30 nm to ≈1 µm.[138] The ability to detect and track single particles in solution also makes it possible to estimate the particle concentration during size characterization. Despite these key advantages with respect to scattering-based size characterization, the higher costs of the equipment, the need of sample concentration or dilution to typically 10^8 to 10^9 particles mL^{-1} (which might differ significantly from the sample concentration required for the intended application), and the required high level of scattering of the particles limit the wide application of NTA. Therefore, DLS still

© 2019 WILEY-VCH Verlag GmbH & Co. KGaA, Weinheim

remains the main technique used for routine size characterization of nanoparticles in liquid.

3.2.4. Electrophoretic Light Scattering

Electrophoretic light scattering is used to estimate the zeta potential ζ of nanoparticles in suspension from their electrophoretic mobility μ_e, defined as $\mu_e = \frac{v}{E}$, where v is the particle velocity and E the externally applied electric field.[139] The zeta potential and the electrophoretic mobility are then related by the Henry equation (Equation (5))

$$\mu_e = \frac{2\varepsilon_r \varepsilon_0 f(KA)}{3\eta} \zeta \tag{5}$$

where ε_r is the relative permittivity of the solution, ε_0 is the permittivity in vacuum, $f(KA)$ the Henry function, and η the viscosity of the solution. Similar to DLS, a laser is transmitted through the measurement cuvette and an electric field is applied to the particle suspension. If the particles are charged, they experience a movement toward the electrode with opposite charge sign with respect to their surface charge. The movement of the particles induces a shift in frequency, a so-called Doppler shift, in the scattered light, which is proportional to the particle velocity.[140] This Doppler shift and the movement direction toward the positive or negative electrode are then used to estimate the electrophoretic mobility of the particles in suspension and, in turn, their zeta potential. However, ζ depends on the particle environment, and the pH and ionic strength of the solution or the particle concentration strongly affect its value.[139] As such, the zeta potential of a suspension of nanoparticles should be characterized under conditions that closely mimic the final working environment of the nanoparticles. Different experimental arrangements have been developed to enable measurements in concentrated samples (>0.01–0.1% v/v), where multiple scattering effects and high solution turbidity would prevent electrophoretic characterization via light scattering detection.[141] Electrophoretic light scattering is often performed with the same instruments that are also used for DLS characterization.

3.2.5. Analytical Ultracentrifugation (AUC)

Analytical ultracentrifugation provides the size, size distribution and density of a suspension of nanoparticles by detecting the sedimentation properties of the nanoparticles when subjected to a centrifugal force.[142] The instrument consists of a high-speed centrifuge equipped with a transparent cell and a detector to monitor the evolution of the dynamic concentration profile of the particles along the cell axis during centrifugation (sedimentation velocity), and the final thermodynamic equilibrium (sedimentation equilibrium).[143] During sedimentation, particles of different size and molecular weight separate and sediment at different rates, therefore multimodal sample distributions can be detected. The extremely high sensitivity of AUC to variations in density and mass of the nanoparticles renders this technique particularly suitable for investigating particle surface coverage.[4,144] Furthermore, the possibility of integrating multiwavelength optical characterization during sample sedimentation largely expands the range of application of AUC in nanoparticle characterization, enabling, e.g., to investigate nanoparticle-protein interaction[145] or particle shape and optical behavior of polydisperse sample populations in a single experiment.[146]

However, data interpretation and translation of sedimentation parameters into size and shape information is not trivial, and can be affected by several factors, such as sample concentration or sample interactions. The high costs of the instrumentation and the long analysis times required, however, strongly limit the widespread application of this technique.

3.2.6. Size Exclusion Chromatography (SEC)

Typically used for the separation and analysis of macromolecules and viruses, size exclusion chromatography is increasingly used for the separation of polydisperse populations of nanoparticles according to their hydrodynamic radius.[147] A SEC separation column is packed with porous microparticles featuring different pore apertures ranging from a few nanometers up to hundreds of nanometers, forming the so-called solid phase of the column. The sample solution, or liquid phase, is then inserted into the column and pressure is applied to make the nanoparticle suspension flow through the column. SEC separation exploits the differential diffusion of nanoparticles into the pore structure of the solid phase: Particles with smaller hydrodynamic radius tend to diffuse more into the porous structure of the solid phase, while larger components of the population travel faster through the column due to shorter diffusion paths and less interaction with the solid phase. Effective sample fractionation is obtained as the liquid phase is eluted from the column. SEC is commonly used in both research and industrial settings for producing highly monodisperse sample populations both in polymer science and biotechnology, e.g., for the separation and analysis of proteins and viruses.[148] Similarly, SEC separation has been widely used for the purification of nanoparticles.[149–151] However, the application of this technique for quantitative analysis and characterization of particle size has numerous limitations. Although particles of known dimensions can be used to calibrate the relationship between elution time and particle size, absolute size quantification and fractionation can be highly challenging.[152] Particles with different surface charges and shape can interact differently with the solid phase, which complicates the prediction and translation of elution times into size information. However, the compatibility of this technique with industrial production and characterization is promoting efforts toward the investigation of SEC separation for quantitative nanoparticle size analysis.[147,152,153]

3.2.7. Field-Flow Fractionation (FFF)

Field-flow fractionation encompasses a class of techniques that use differential transport of nanosized objects along a microchannel for separation and characterization. The sample is introduced in a channel featuring a parabolic laminar-flow

© 2019 WILEY-VCH Verlag GmbH & Co. KGaA, Weinheim

profile and a force perpendicular to the flow direction is then applied, which induces sample accumulation against one channel wall. Due to sample diffusion, a concentration gradient is generated across the cross section of the transport channel. Particle diffusion is dependent on the hydrodynamic radius, therefore particles of different dimensions establish different concentration gradients in the channel cross section. These gradients of distributions ultimately result in different mean transport velocities and elution times of particles with different sizes.[154] The perpendicular accumulation force, flow velocity and channel dimensions can be tuned to change the resolving power of the FFF separation. FFF can provide absolute size quantification if the relationship between the elution time and the applied force is known or can be calibrated using standards. In addition, the technique can be used to separate the sample population and generate monodisperse distributions of particles for downstream analysis. The low shear stresses experienced by the particles and the tunable selectivity of the FFF analysis have rendered this technique a commonly used analysis method for investigating nanoparticle populations.[155]

As different forces can be applied to induce sample accumulation at the channel wall, FFF has been used to investigate different physicochemical properties, such as magnetic susceptibility by use of magnetic gradients, dielectric properties by applying external electric fields, or particle composition by applying thermal gradients or sedimentation forces.[156] However, FFF is typically used for size-based separation and investigation of polydisperse samples. The most common FFF technique is flow field-flow fractionation (usually referred to as FIFFF), which exploits a perpendicular cross-flow to induce a drag force for driving the particles toward the accumulation wall. This perpendicular force is proportional to the cross-flow velocity u, the fluid dynamic viscosity η and the particle hydrodynamic radius R_h, as defined by Stokes' law $F = 6\pi\eta R_h u$.[157] Porous membranes at the channel walls allow fluid to exit perpendicular to the axial transport direction, while retaining particles within the separation channel. According to the configuration of the cross flow and used porous membrane, FIFFF is further divided in different subtechniques, with hollow-fiber FIFFF (also known as HF5) and asymmetric-F1FFF (AF4) being the most commonly used techniques for routine analysis.

3.2.8. Fluorescence Correlation Spectroscopy (FCS)

Fluorescence correlation spectroscopy and fluorescence cross-correlation spectroscopy (FCCS)[158,159] rely on the detection of emitted light rather than scattered light. As fluorophores diffuse in and out of the confined volume of excitation light in a confocal microscopy setup, they emit fluorescent light, and the resulting intensity fluctuations of the emitted light are recorded by a detector. Similar to DLS, the intensity fluctuations can be used to generate an autocorrelation or cross-correlation function which in turn allows for extracting translational diffusion coefficients, and the diffusion coefficients themselves depend on the hydrodynamic particle size.[160,161] At the same time, the amplitude of the signal depends on the number of fluorophores present in the excitation volume. Besides determining diffusion coefficients, the techniques can also be used to investigate chemical rate constants, molecular concentrations, or—especially in the case of FCCS—binding events in complex systems that do not cause a significant change in mass and hence in diffusion properties.[162] Typically, the concentration should be rather low (on the order of 5 molecules at any given time in the excitation volume), and the technique is especially useful for characterizing small, dynamic systems.

3.2.9. Tunable Resistive Pulse Sensing (TRPS)

Tunable resistive pulse sensing is a technique for the characterization of size, zeta potential and concentration of particles in suspension with single-particle resolution and in complex medium conditions.[163] TRPS is based on the Coulter principle, which measures the variation of ionic current through a pore due to partial blocking of the pore aperture caused by the passage of a particle. As such, TRPS requires the use of conductive solutions for the analysis. However, this requirement renders this technique compatible with the characterization of nanoparticles under physiological buffer conditions for investigating the fate and interactions of nanoparticles in complex media.[164] TRPS differs from standard resistive pulse measurements, as the pore aperture can be tuned by stretching the pore-containing membrane. The tunability of the pore aperture enables both to clear the pore in the case of clogging, as well as to adapt the measurement sensitivity during acquisition.[165] Equation (6) describes the flux of particles (particles m^{-2} s^{-1}) through the pore[165]

$$\boldsymbol{J} \approx \left(\boldsymbol{J}_{ep} + \boldsymbol{J}_{eo}\right) + \boldsymbol{J}_{pdf} = \frac{C\varepsilon}{\eta}\left(\zeta_{part} - \zeta_{pore}\right)\boldsymbol{E} + \frac{C}{A}\boldsymbol{Q} \tag{6}$$

where $\boldsymbol{J}_{ep}$ and $\boldsymbol{J}_{eo}$ represents the electrophoretic and electroosmotic fluxes generated by the electric field $\boldsymbol{E}$, respectively, and $\boldsymbol{J}_{pdf}$ indicates pressure driven flux with volume flow rate $\boldsymbol{Q}$. C indicates the particle concentration, and ε and η are the solution permittivity and viscosity. Finally, ζ_{part} and ζ_{pore} are the zeta potential of the particle and pore, respectively.

From Equation (6), when $\boldsymbol{J}_{ep}$ and $\boldsymbol{J}_{eo}$ are negligible with respect to $\boldsymbol{J}_{pdf}$, particle concentration can be measured by calculating the rate of recorded events, if the pressure-driven flow is known. The amplitude of the induced current variations carries information on particle size and scales with the ratio of particle size and pore aperture. Furthermore, investigation of the induced-peak shape can also provide information on particle shape and anisotropy.[166] Finally, TRPS can also be used to measure the surface charge of particles in solution. This property can be obtained either by varying the applied pressure and measuring the electric field across the pore so that $\boldsymbol{J} = 0$, or, if $\boldsymbol{J}_{pdf}$ is known from calibration, by estimation from the particle velocity, which is proportional to the width of the induced peak.[165] This latter method, in particular, enables to obtain single-particle surface-charge measurements.

Although it is generally assumed that the signal amplitude scales linearly with the particle volume, this relationship deviates from linearity when the particle size approaches that of the pore aperture or for highly stretched pores, which might feature a nonpredictable aperture shape and size.[163] As these effects

© 2019 WILEY-VCH Verlag GmbH & Co. KGaA, Weinheim

are difficult to model with precision, the use of calibrated particles of different dimensions can be used to characterize the response of TRPS for samples of different sizes.

3.3. Advanced Techniques

The advanced techniques presented here are of interest for the characterization of specific properties of nanoparticles and of their behavior, which cannot be accessed using standard characterization methods. The methods discussed in this section are summarized in **Table 3**.

3.3.1. In Situ Liquid-Cell (LC) and Atomic-Resolution (AR) TEM

As discussed previously when presenting the dry-state characterization techniques, TEM is a unique and powerful characterization method, however normally restricted to samples in dry state. In situ liquid-cell TEM has been developed to overcome this major limitation.[167] Here, a nanoparticle suspension is sandwiched between two electron-transparent windows and the system is hermetically sealed to protect the liquid from the vacuum environment of the TEM[168–170] (**Figure 8**a). This technique makes it possible to image previously "unobserved" processes such as nucleation and growth of nanoparticles as well as their interaction and assembly.[168,171] The power of LC TEM has been demonstrated by studying several aspects of synthesis and use of gold nanoparticles, namely their nucleation rates,[172] and the dynamics and assembly between bare and functionalized particles (Figure 8b).[173–176] Finally, atomic-resolution transmission electron microscopy (AR-TEM) enables the study of dynamic processes and provides real-time observation of changes at the molecular level with atomic sensitivity.[177,178] The first study in 2007 reported AR-TEM movies of conformational changes of a single hydrocarbon molecule.[179] The use of this technique for nanoparticles is just at the beginning, but it opens interesting avenues, such as the investigation of nanoparticle-protein interactions.[177]

3.3.2. Electron Cryo-Microscopy (Cryo-EM)

Electron cryo-microscopy fills an important gap, as it allows direct imaging of biological nanoparticles that cannot be dried without damage.[180] Such nanoparticles are abundant in nature, e.g., protein/RNA complexes, organelles, and viruses.[181] However, also artificial nanoparticles can be challenging to dry without affecting their stability, as it is often the case for liposomes and many types of drug formulations. The field of cryo-EM has been transformed by a series of breakthroughs in hardware development and computational methods over

Table 3. Summary of advanced characterization methods.

Technique	NP[a)] state	Parameters	Advantages	Limitations	Reviews
LC- and AR-TEM	In solution	*Size* (atomic to ≈100 nm) *Shape* (2D projection) *Dynamics*	Single-particle and atomic resolution, imaging of dynamic processes	Extremely low throughput, high costs, highly trained users	[170]
Cryo-EM	Flash-frozen solution	*Size* (<1 to ≈100 nm) *Shape* (2D projection and 3D reconstruction)	No drying or staining required, compatible with materials sensitive to e-beams	Very low signal-to-noise ratio, high costs, highly trained users	[82,181,183]
Electron tomography	Dry and in solution	*Size* (<1 to ≈100 nm) *Shape* (3D imaging)	3D imaging of individual nanoparticles	Extremely low throughput, high costs, highly trained users	[53,187]
NMR cryoporometry and DSC thermoporosimetry	In solution (freezing and thawing)	*Pore aperture* *Pore volume*	Investigation of pore volume and volume accessible to solvents in solution	Limited throughput, ensemble-based	[194]
Super-resolution microscopy	Dry and in liquid	*Surface coating* *NP structure and behavior*	Selectivity provided by fluorescent tag, can be performed on dynamic systems	Limited optical (>30 nm) and temporal (50–100 ms) resolution	[199]
Single molecule fluorescence microscopy	In liquid	*Pore structure* *Pore functionalization*	Information on the internal porous structure of materials	Host material must have low autofluorescence, dye has to be able to diffuse inside the porous structure	[204,205]
Nanomechanical resonators	Dry and in suspension	*Mass* *Density* *Size* (indirect)	Information on composition, size and interactions with the solvent	Low throughput, not always possible to obtain single-particle characterization	

[a)]NP stands for nanoparticle.

© 2019 WILEY-VCH Verlag GmbH & Co. KGaA, Weinheim

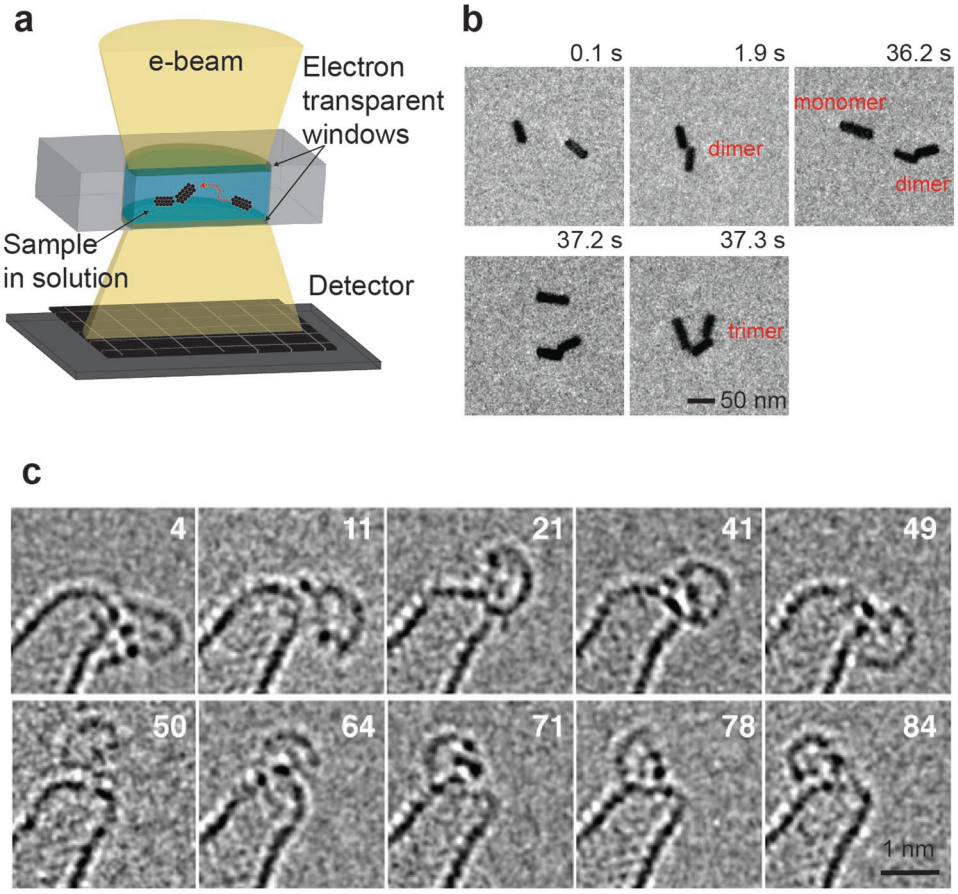

Figure 8. LC-TEM and AR-TEM. a) A nanoparticle suspension is sandwiched between two electron-transparent windows (e.g., made of thin silicon nitride) to prevent the evaporation of the solution in the high vacuum environment during TEM imaging; b) formation of gold nanorod chains by sequential attachment of nanorods in solution. Adapted with permission.[176] Copyright 2017, American Chemical Society; c) conformational changes of a biotinylated molecule grafted to the tip of a tapered single-walled carbon nanotube. The number refers to the frame number extracted from the TEM movies. Adapted with permission.[178] Copyright 2015, American Chemical Society.

the past decade. Although the attainable resolution is strongly sample dependent, values down to 2 Å have been reported,[182] while values better than 10 Å are achieved relatively routinely today.[183]

Ice crystallization constitutes the biggest risk for the integrity of the structure when samples are prepared for cryo-EM. To prepare samples that are frozen amorphously, or vitrified, for TEM analysis, a few microliters of a suspension are applied to a TEM grid, blotted in a humidified chamber to leave a water film only ≈100 nm thick, and flash frozen by plunging the grid into liquid ethane or propane at high speed (**Figure 9**a).

TEM is then used to obtain 2D projection images of the nanoparticles embedded in vitreous ice. These images often have very low contrast, as the electron density in organic materials differs only weakly from the solvent (Figure 9b).[181,184] When the particles are identical, such as certain types of viruses or protein complexes, analysis algorithms are able to reconstruct the 3D structure from a large set of images of randomly oriented single particles. When the particles are not identical, the projection images still provide valuable information about their inner structure, size, and size distribution. If the material can tolerate a higher electron dose, tilt-series can be acquired to enable reconstruction of the 3D-structure of individual particles by cryo-electron tomography (cryo-ET).[82,181]

Another valuable technique is cryogenic scanning electron microscopy (cryo-SEM). Because the signal in SEM emerges mainly from the surface of the sample, different preparation techniques than in cryo-TEM are required to access nanoparticles embedded in vitreous ice. Vitrified samples for cryo-SEM are often made by high-pressure freezing, which is able to yield amorphous ice specimens up to several hundred micrometers thick. To expose the inner structures, one approach is to fracture the vitrified blocks in a method known as freeze fracture. Alternatively, focused ion beam (cryo-FIB) milling or cryo-ultramicrotomy can be used to make serial sections. An important advantage of cryo-SEM is that the cost for the instruments is significantly lower than for TEM. The wide field of view of the SEM is useful for observing the interaction of nanoparticles with larger objects, such as whole cells. However, the attainable resolution rarely exceeds 1 nm and does not provide the detailed insight into the molecular structure that modern cryo-TEM can achieve.[181]

© 2019 WILEY-VCH Verlag GmbH & Co. KGaA, Weinheim

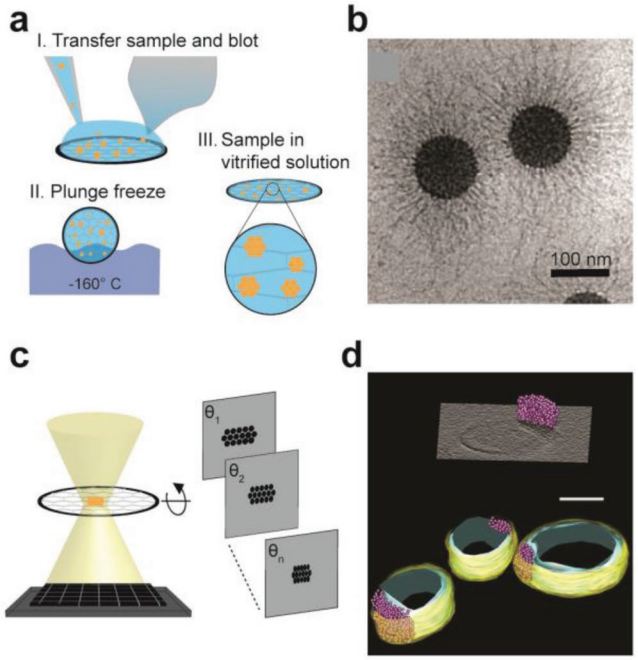

Figure 9. Cryo-EM and electron tomography. a) Main steps required for sample preparation for cryo-EM; b) spherical nanoparticles formed by a poly(styrene) core with grafted chains of poly(styrene sulfonate acid). Cesium ions and bovine serum albumin were used to enhance the image contrast of the brush layer. Reproduced with permission.[184] Copyright 2005, American Chemical Society; c) to perform electron tomography, different EM micrographs are obtained by varying the angle between the sample and the incident EM beam; d) Cryo-EM tomogram revealing the localization of clusters of superparamagnetic iron oxide nanoparticles (purple) within the bilayer of liposomes (yellow/green). Scale bar 50 nm. Reproduced with permission.[188] Copyright 2014, American Chemical Society.

3.3.3. Electron Tomography

Conventional microscopy provides a 2D projection of a 3D object. Therefore, information such as shape, thickness or uniformity (e.g., spatial dimension) of nanoparticles can only be roughly estimated, and the interpretation of the projection of complex nanoparticles is quite challenging and can lead to incorrect conclusions. Hence, more information is needed to make reliable statements about the 3D structure of the investigated samples.

Tomography is the best approach to provide 3D information of objects. This method is based on the acquisition of multiple 2D projections of the sample at different angles relative to the incident beam, and on the reconstruction of a 3D representation from these partial images[185] (Figure 9c). Tomography has been originally developed for X-ray analysis and is nowadays a widely used approach in medicine (computed tomography), but it is not suitable for nanoparticle analysis.

Electron tomography is the technique of choice for studying the 3D structure of a nanoparticle (Figure 9d).[186–188] Recently, this method could be expanded to study individual nanocrystals in solution.[52] However, electron tomography has several important limitations such as poor statistics, very low throughput (a single nanoparticle 3D visualization can require about one day of data acquisition and multiple days of data processing and 3D reconstruction), and a high level of complexity (especially the tomographic reconstruction of the 3D image), which limit this technique to highly trained specialists. In addition, particle drift and beam damage induced changes of the object during the investigation have to be taken into account during the reconstruction and rendering of the 3D image.

3.3.4. NMR Cryoporometry and DSC Thermoporosimetry

Liquids confined within nanometer-sized pores experience a decrease in freezing and melting temperature with respect to their bulk counterparts as a consequence of the extremely high surface-to-volume ratios of the confined crystals and the imposed surface curvature.[189,190] Measuring the variations of the temperature of phase changes provides direct information on the volume and the dimensions of the pores accessible to the liquid[191] (**Figure 10**a). Although both freezing and melting phase changes can potentially be used for such a study, detection of melting temperatures is usually preferred to avoid uncertainties arising from supercooling effects. These transition temperatures can be measured with high precision using either differential scanning calorimetry (DSC) thermoporosimetry[192] or nuclear magnetic resonance (NMR) cryoporometry.[193,194] With respect to commonly used gas sorption techniques to measure the pore windows and the pore sizes, NMR and DSC measurements are carried out in liquid and no drying of the sample that could potentially affect the nanoparticle framework is required. This is particularly important when detecting the pore size and pore size distribution of delicate structures envisioned to work in liquid environments, such as hydrogel nanoparticles[195] or porous biopolymeric nanoparticles.[196] Furthermore, the ability to probe nanoparticles directly in solution enables studying dynamic variations in the porous structure of the nanoparticles when exposed to different solvent conditions (Figure 10b).[197]

3.3.5. Super-Resolution Microscopy

The ability of providing dynamic information with spatial resolution below the conventional diffraction limit of optical microscopy has rendered super-resolution microscopy, or nanoscopy, an essential tool in cell and tissue biology research.[198] Spatial resolution below the diffraction limit is achieved by employing acquisition strategies to improve the localization of single emitting fluorophores (such as photoactivated localization microscopy or stochastic optical reconstruction microscopy) or by reducing the size of the point-spread function of the emitted light (such as stimulated emission depletion or structured illumination microscopy) (**Figure 11**a). Recently, super-resolution microscopy has also found applications in material science for providing superior optical characterization of samples under investigation.[199] Although higher spatial resolution can usually be obtained by electron microscopy or scanning probe microscopy, fluorescence-based characterization can provide higher selectivity, higher contrast and nonsuperficial characterization, depending on the fluorescent labeling strategy employed. Examples of such enhanced selectivity and

© 2019 WILEY-VCH Verlag GmbH & Co. KGaA, Weinheim

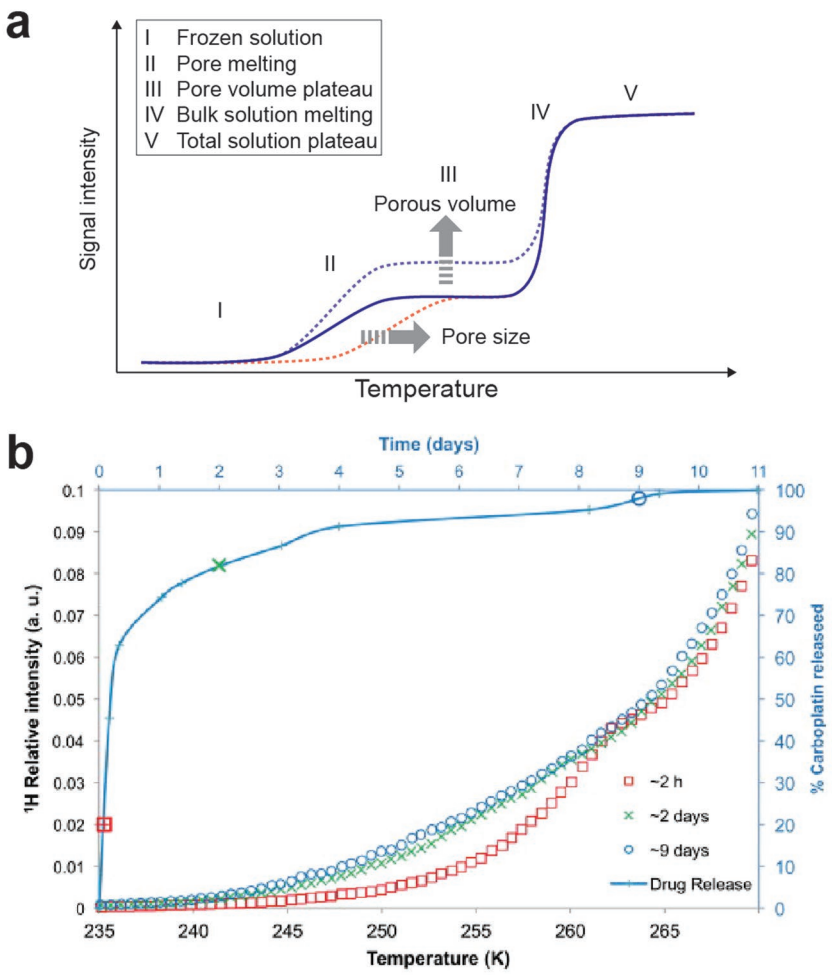

Figure 10. NMR cryoporometry. a) An ideal NMR cryoporometry curve reporting the main curve features; b) melting curve of porous polymer nanoparticles loaded with Carboplatin drug after different incubation times in artificial cerebral spinal fluid. The NMR cryoporometry curves show an increase in small pores and total pore volume within the first 2 days, which corresponds to a burst release of drug in solution. Reproduced under the terms of the CC-BY license.[197] Copyright 2014, the Authors. Published by Elsevier.

nonsuperficial characterization are the visualization of the hollow nature of lipid coated nanocapsules,[200] the characterization of the internal compartmentalization of core–shell microgels,[201] the swelling and contraction of microgel nanoparticles (Figure 11b),[202] and the penetration and adsorption of fluorescently labeled proteins with different molecular weights into the framework of mesoporous silica nanoparticles with different pore sizes (Figure 11c).[203]

3.3.6. Single Molecule Fluorescence Microscopy

Single molecule fluorescence microscopy and tracking can be used to obtain valuable information about the porous system and the host-guest interactions of nanomaterials.[204,205] The dynamics of guests inside porous nanoparticles, and the interactions of the guests with the walls of the nanoparticles are sometimes the key for the targeted application. Examples of the application include the investigation and mapping of the internal porous structure and defects of porous nanomaterials by following the diffusional movement of fluorescent dyes inside the pores (Figure 11d),[206–208] or the determination of the diffusion coefficients of dyes and oligonucleotides inside a porous nanomaterial in dependence of the functionalization of the pore walls.[209–211] The latter can give detailed information on how the presence and density of functional groups on the pore walls affect the diffusional movement of the guest molecules, for example through electrostatic interactions.

3.3.7. Nanomechanical Resonators

Micromechanical resonators present a characteristic resonance frequency which depends on the oscillating mass of the resonator. Thanks to the extremely low inertial masses of nano- and micron-sized resonators (attogram to nanogram inertial mass) and the high quality factors, adsorption of particles on the surface of a resonator causes a detectable shift in resonance frequency, proportional to the mass of the adsorbed particle. This nanomechanical-based mass spectrometry has enabled the characterization of mass of single intact nanoparticles regardless of the ionization state of the sample, allowing the mass measurement of neutral particles in the Megadalton to Gigadalton regime, which is not possible with standard mass spectrometry approaches.[212,213] This method of detection can be extended to colloidal suspensions by embedding a microfluidic channel into the resonator to enable particles in solution to cross it, while retaining its oscillation in a vacuum environment.[214] These devices, called suspended microchannel resonators, have enabled the characterization of samples of gold nanoparticle mixtures ranging from 10 to 20 nm in diameter, with single-particle detection capability.[215] By allowing multiple particles to flow simultaneously through the embedded channel and by employing an autocorrelation analysis of the time-domain mass signal, the resolution of these devices could be extended to the characterization of nanometer-sized polymer particles.[216] This technique, called Nanomechanical Mass Correlation Spectroscopy, was used to investigate the complex partitioning of binary solvent mixtures within the framework of mesoporous metal-organic framework (MOF) nanoparticles with different surface functionalization (**Figure 12**).[217] The particles exhibited different effective densities in solution as a function of pore functionalization and solvent composition, indicating that the local microenvironment within the pore structure of porous nanoparticles might not reflect the bulk solvent composition.

© 2019 WILEY-VCH Verlag GmbH & Co. KGaA, Weinheim

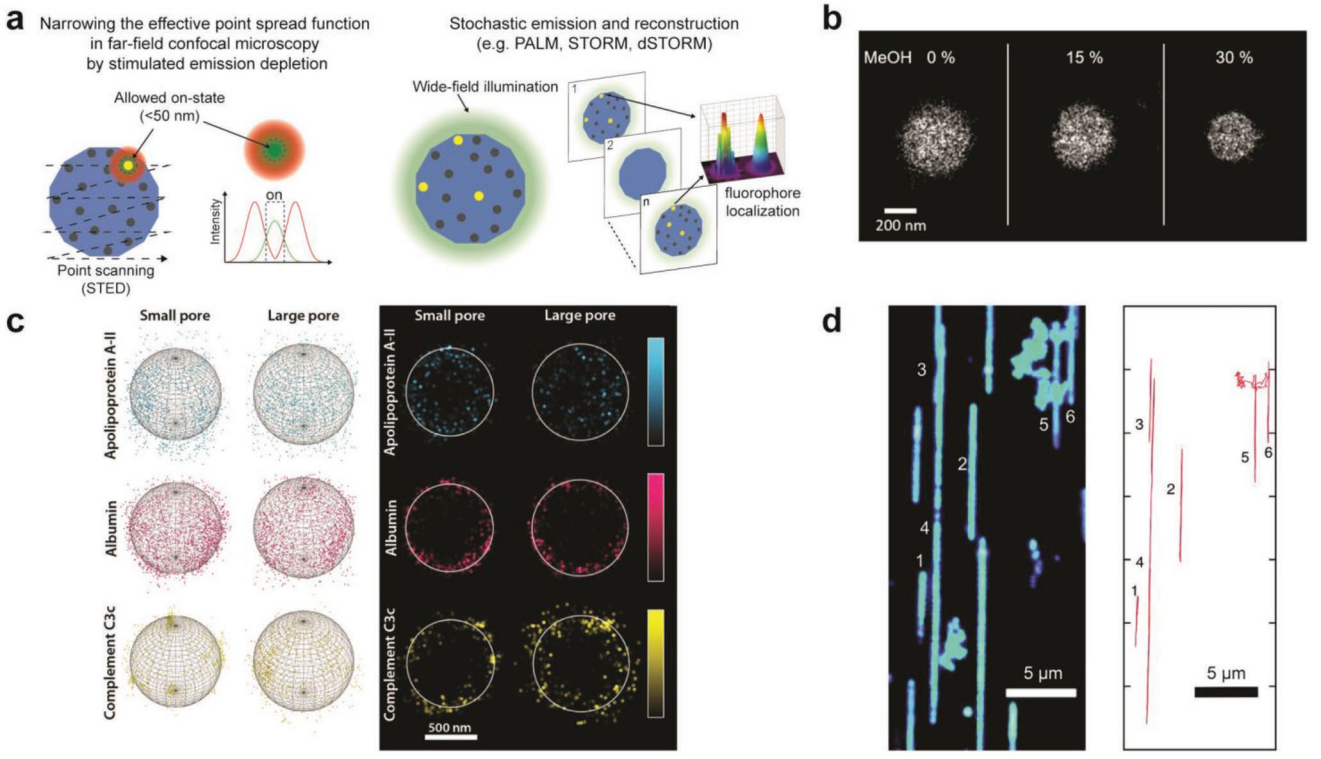

Figure 11. Super-resolution microscopy and single molecule fluorescence microscopy. a) Different methods to achieve optical resolution below the diffraction limit. In STED microscopy (left), a doughnut-shaped light pattern (red) is used to suppress the emission of excited fluorophores (green) in an annulus via stimulated emission ("off" state). The emitting region is thereby confined to a subdiffraction-sized spot at the center of the doughnut. In STORM microscopy (right), only a sparse collection of randomly distributed fluorophores is turned on at any time by a low-intensity wide-field excitation Single molecules are localized with subdiffraction accuracy. This process is repeated for multiple images to reconstruct the complete object; b) contraction of fluorescently labeled microgel nanoparticles upon addition of methanol in solution visualized by dSTORM. Reproduced with permission.[202] Copyright 2016, Elsevier; c) adsorption of different labeled proteins on the surface and within the porous structures of mesoporous silica nanoparticles featuring pores of different size. On the left, the sphere of best fit as calculated from the STORM images. On the right, the fluorescence data are flattened and their distribution is plotted in 2D. Reproduced with permission.[203] Copyright 2017, American Chemical Society; d) left: "maximum projection" overlay of the individual frames of a movie that shows single dye molecules diffusing inside the pores of a mesoporous silica thin film. Right: The underlying porous structure was reconstructed by fitting each single molecule in each frame and linking them together to form trajectories. The trajectories show the real pore structure, including pore alignment and defects, and can also be used to extract dynamic information such as the diffusion coefficient of the dye inside the porous host. Reproduced with permission.[207] Copyright 2012, American Chemical Society.

4. Nanoparticle Characterization Overview

Nanoparticle characterization is generally motivated by the requirements of specific applications. Such requirements are often given in the form of safety regulations or quality control standards. If the application does not already prescribe a specific set of characterization techniques, some general guidelines can be considered. Here we aim to provide some general recommendations to help with the selection of methods in a wide range of applications. As a starting point, the flowchart in **Figure 13** provides a framework organizing the most important techniques described in this article into groups and key questions to help the reader decide which techniques are most suitable for the sample under investigation. Although it is not possible to provide a comprehensive overview of all techniques for all types of samples, we believe that this workflow can be applied to many typical cases of nanomaterials.

Nanoparticle characterization techniques can be categorized as targeting solid samples or powders, shown on the left side of the flowchart, or suspensions, featured on the right.

Solids and powders often come as aerosols or as particles deposited on a surface from a suspension. These samples provide considerable freedom for studying size distribution and particle morphology by electron microscopy, atomic force microscopy, X-ray scattering, or mass spectrometry. Dry samples can be characterized in air or vacuum where no solvent molecules interfere with the measurement.

In most situations, electron microscopy is the method of choice for dry samples because the technique is extremely versatile, precise, relatively simple to use (especially SEM), and widely available. Unfortunately, nonconducting samples accumulate charge and often deform slowly in the electron microscope. Beam-sensitive samples need to be coated with a thin conducting layer (typically platinum, gold, or graphite) or analyzed at elevated pressure by environmental SEM at a low dose. TEM analysis of nonconducting samples also requires attention to the same issues of beam damage and charging.

When electron microscopy cannot be used, AFM can be considered as an alternative. On the one hand, AFM analysis lacks many of the material contrast and elemental analysis options

© 2019 WILEY-VCH Verlag GmbH & Co. KGaA, Weinheim

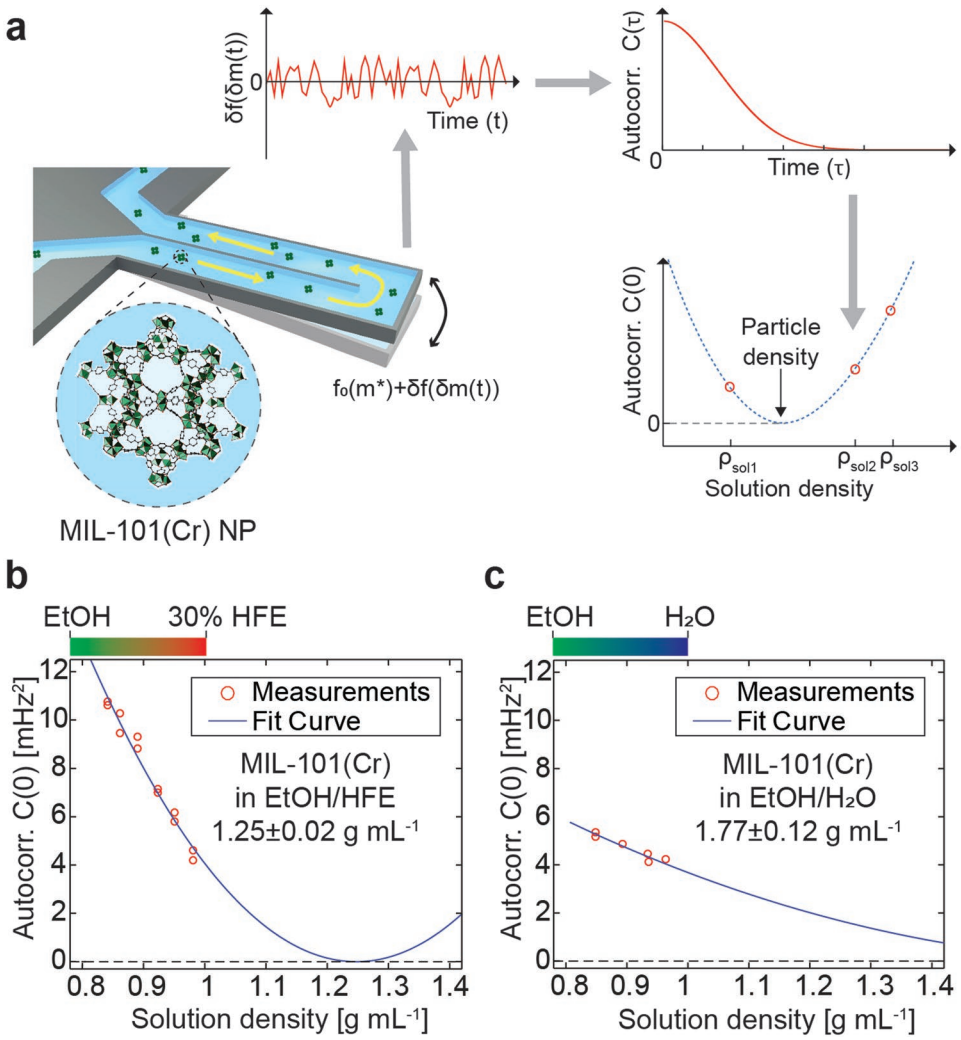

Figure 12. Nanomechanical mass correlation spectroscopy. a) The detection principle of nanomechanical mass correlation spectroscopy. Particles flowing through the microfluidic channel embedded in a mechanical resonator induce transient fluctuations to the resonant resonance frequency, which are proportional to the particle buoyant mass. An autocorrelation analysis of the time-domain signal is used to enhance the particle contribution with respect to the uncorrelated noise background; b,c) MIL-101(Cr) porous nanoparticles were suspended in binary mixtures of different polarities to investigate the dependence of the particle density to the composition of the solvent mixtures. (a–c) Reproduced under the terms of the Creative Commons Attribution-NonCommercial license.[217] Copyright 2018, The Authors. Published by Wiley-VCH.

offered by SEM. AFM also has lower throughput and can be challenging to perform, as particles that are not stably attached to a surface can be easily dislodged by the scanning AFM tip. On the other hand, AFM provides sub-nanometer topographic resolution and can be used to analyze mechanical properties.

SAXS provides less detail than microscopy in terms of the size distribution and morphology. Scattering patterns are generated from large populations of particles. Although it is possible to extract information about heterogeneity and aggregation of nanoparticles from the scattering patterns, the level of detail to expect does not match the fine grained size distribution and morphology that can be extracted from analyzing electron microscopy images or AFM images.

For the characterization of biological nanoparticles, the molecular weight is often more relevant than physical size or morphology. Mass spectrometry is becoming an excellent tool even for large particles. Long reserved for low molecular weight compounds, this technique now is able to access the range of large macromolecular complexes in the Megadalton range and even beyond. However, the measurement is based on the mass-to-charge ratio and provides limited information on the actual size and morphology of the particles.

Measuring the surface area of nanoparticles is straightforward by gas sorption analysis when particles come in the form of a dry solid or a powder.

Nanoparticle suspensions are more challenging to analyze by microscopic methods than dry samples. In liquids, electron microscopy is only an option in a few cases where liquid cell TEM can be used. However, liquid cell TEM is still largely at a developmental stage. For most users today, AFM will be the only routinely available method that is able to image nanoparticles in liquids with nanometer resolution.

In choosing alternative characterization methods for suspensions, it is first advisable to consider the expected degree

© 2019 WILEY-VCH Verlag GmbH & Co. KGaA, Weinheim

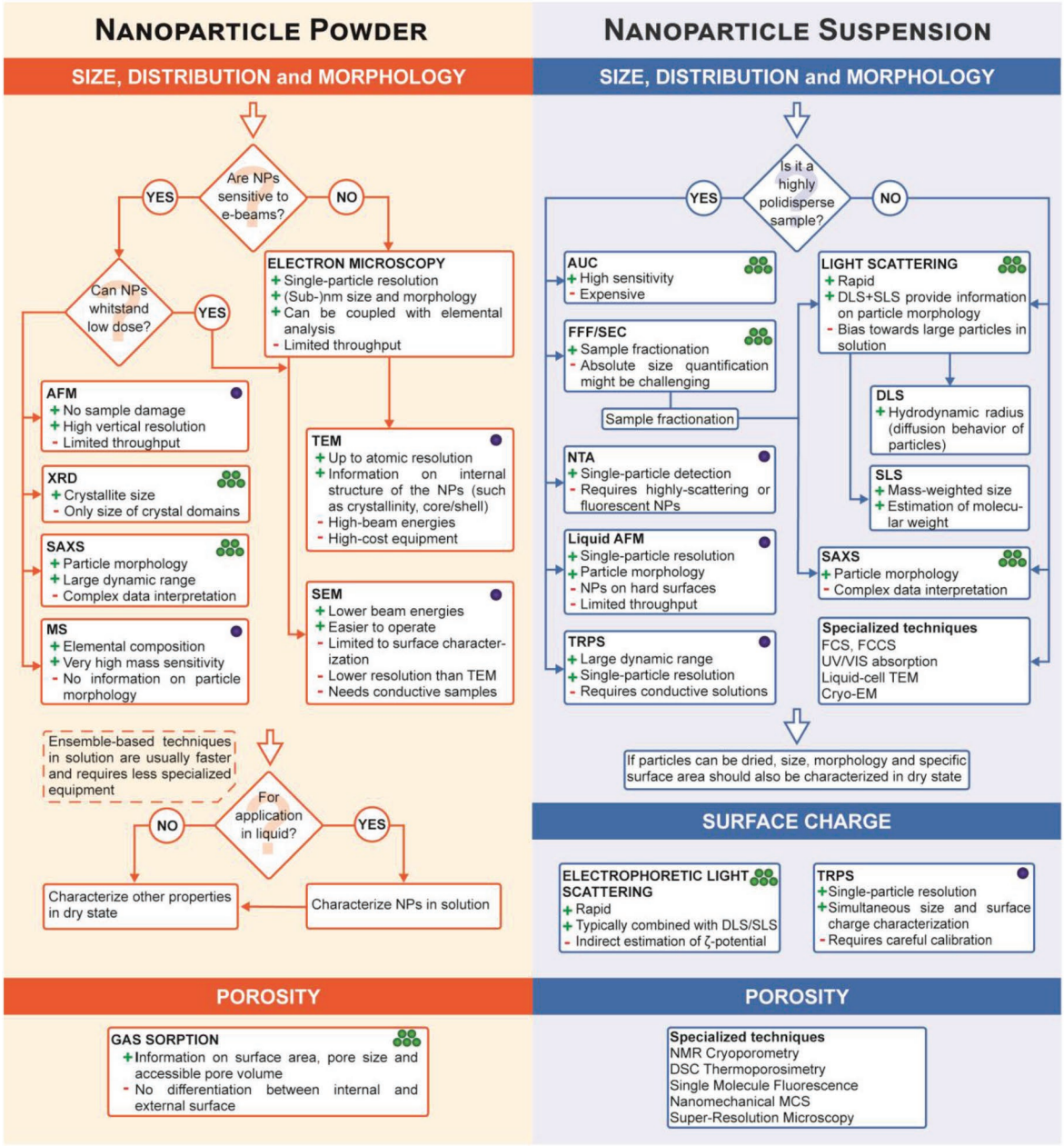

Figure 13. Flowchart. Flowchart depicting the main steps for the characterization of size, size distribution, morphology, surface charge, and porosity of nanoparticles, both in dry state and in solution. NP stands for nanoparticle.

© 2019 WILEY-VCH Verlag GmbH & Co. KGaA, Weinheim

of polydispersity. The answer to this should be followed by a critical assessment whether the target application requires the discrimination of all populations within the sample or not. If the sample is highly polydisperse, with diameters spanning more than one order of magnitude, then techniques on the left branch of the flowchart for suspensions in Figure 5 are usually preferable. The reason for this is that otherwise there is a risk of obtaining results that are skewed by outliers, which can affect the measurement even if their population is very small.

Methods that are well suited for the characterization of polydisperse suspensions operate either by detecting particles one-by-one or by first separating the mixture into subpopulations, sometimes referred to as bands or subensembles, which are themselves made up of large numbers of particles with more homogeneous characteristics.

Among the most established techniques that operate by separation are analytical ultracentrifugation, field-flow-fractionation, and chromatography. There are two potential caveats when using these methods: first, if the nanoparticles are in a dynamic equilibrium, then separation can perturb this equilibrium and may lead to misleading results. Second, the detection sensitivity may be insufficient for some of the less-numerous subpopulations in the ensemble. If this is the case, one can consider collecting fractions of the separated sample and subjecting these fractions to light scattering, SAXS, or more specialized analyses.

Methods for single nanoparticle characterization in liquid have become commercially available only relatively recently. Their physical principles are diverse, but all exploit the mobility or the difference in conductivity/density to the surrounding liquid. Thus, the solvent environment is an integral part of the measurement. With this in mind, NTA, TRPS, and nanomechanical resonators are powerful tools for the characterization of nanoparticle suspensions. The main limitation of all three techniques is their relatively limited throughput. Which of the three techniques is most appropriate depends on the specific characteristics of the sample and should be decided case by case based on the application examples provided in the detailed overview presented before.

Other important characteristics of nanoparticles in suspension besides the mean size, size distribution, and morphology are the surface charge and surface area, including the area inside of pores. Characterization of surface charge is most commonly performed by electrophoretic methods, but it is important to note that TRPS, by the very nature of the method, is also sensitive to surface charge. Porosity is a more challenging parameter to quantify in solution. Note, however, that this is not only due to the limitations of measurement technology. Especially for microporous and mesoporous materials (pore sizes <2 and 2–50 nm, respectively), the accessibility of pores can differ for bulky solvent molecules or bulky solutes. Therefore, it is important to consider carefully what is being measured by the techniques available.

In summary, the choice of methods is typically a compromise between the demands of the application and the restrictions of the different techniques. As a rule, first the simplest techniques should be applied to obtain answers to some key questions. However, the quantitative results at this initial stage should also be treated with a healthy degree of skepticism. The rich detail contained in electron micrographs is well suited to inform subsequent decisions regarding polydispersity, drying artifacts, and beam sensitivity. This information forms a basis for deciding if and how subsequent analyses should be performed, and we suggest that the flowchart in Figure 13 is used as a guide in this process.

4.1. Assessment of Multifunctional Efficiency of Nanoparticles

To assess the efficiency and functionality of nanoparticles, we have to consider the ratio of functional and nonfunctional components, and the number of synthetic steps required to produce these multifunctional products. We recently suggested to evaluate the synthesis of functional nanoparticles not only based on yield and product selectivity (e.g., atom economy) but also with regard to the specific tasks the nanoparticles can fulfill (number of functional units) and the simplicity of the production process (number of process steps)[18]

$$\mathrm{FR}:=\frac{n_{\mathrm{FU}}}{m_{\mathrm{BU}}} \tag{7a}$$

$$\mathrm{PE}:=\frac{n_{\mathrm{FU}}}{r_{\mathrm{PRS}}} \tag{7b}$$

$$\mathrm{MFE}:=\mathrm{FR}\cdot\mathrm{PE}=\frac{n_{\mathrm{FU}}^{2}}{m_{\mathrm{BU}}\cdot r_{\mathrm{PRS}}} \tag{7c}$$

The functionality ratio (FR; Equation (7a)) of a nanoparticle is defined as the number of functional units (n_{FU}) divided by the total number of building units of the nanoparticle (m_{BU}). The process efficiency (PE, Equation (7b)) of a nanoparticle synthesis is defined as the number of functional units (n_{FU}) divided by the number of process steps (r_{PRS}). Finally, the multifunctional efficiency (MFE, Equation (7c)) involves both parameters FR and PE and results in a quantity that values both a high degree of functionality and a facile manufacturing process. The key advantage of this concept is that a functional nanoparticle (e.g., nanocarrier) can be evaluated from the economic and synthetic viewpoint before the expensive and time-consuming biological assessment takes place.[18]

5. Conclusions

The growth of nanoparticle material classes and their application to tackle global problems of our time requires progresses in nanoparticle characterization. The four properties *size*, *shape*, *surface charge*, and *porosity* of nanoparticles are intimately connected with their functionality and their effects on health and the environment. Measuring these properties is important for translating potential benefits of nanomaterials into specific applications. Characterization is also the first step to ensure that synthesized compounds possess the desired properties and that the properties of different batches are reproducible.

To be able to correlate the physicochemical properties of the nanoparticles with their performance in a specific task,

© 2019 WILEY-VCH Verlag GmbH & Co. KGaA, Weinheim

characterization needs to be both accurate and precise. Therefore, standardized standard operating procedures should be developed to improve the comparability of results between different materials and laboratories. It is crucial that new data can be compared and evaluated with previously published results in a meaningful way. This will require conclusive and harmonized analytical protocols to be applied worldwide.

We wish to give the following general recommendations for nanoparticle characterization:

1. Consider the intended form the target application of the nanoparticles. The form (colloidal suspension or solid powder) often dictates the need for the specific characterizations that should be used.
2. Place reasonable bounds on the precision and statistical confidence with which physicochemical properties need to be measured to satisfy the needs of the application. For example, the statistical demands in the quality control for pharmaceutical formulations will typically be higher than for industrial coating materials.
3. Develop or adopt standard characterization and standard operating procedures to be systematically and thoroughly followed for *every* batch.
4. The protocol used to measure the physicochemical parameters as well as the meta-data should be described in detail. Besides a detailed description of the experimental protocol, the experimental parameters, and method-specific settings that were used, this should include how the data were analyzed (e.g., what model was used to obtain a certain value).
5. In the case of suspensions, the exact chemical composition of the liquid matrix should be specified. Both pH and ionic strength should be measured and reported for aqueous solutions.
6. Measured parameters should be calibrated against a standardized reference. If no standardized references for a quantitative comparison with the nanomaterial at hand are available, internal references can be used to, at least, ensure consistency between batches. For example, obtaining similar size distributions from different nanoparticle batches and/or a constant reference sample should ensure the reproducibility of results.
7. Whenever feasible, more than one technique should be used to characterize the same quantity.
8. The obtained results should be compared with published data whenever feasible.

The development of inexpensive analytical methods should be an integral part of future research. At the same time, existing techniques should be improved and their current boundaries and limitations expanded. In particular, novel techniques are needed for cross-validation, and to measure physicochemical properties that are currently difficult to test. Especially the identification of the interaction of ions and/or molecules inside the internal volume of porous nanoparticles in a liquid medium is so far a largely underexplored topic. Another important aspect is the characterization of nanoparticles under the envisioned operating conditions of the nanomaterial. One important lesson learned in the last decade is that in biological fluids proteins assemble with the nanoparticles, leading to a protein corona that gives a "biological identity" to the particles.[20,218] As the application of nanoparticles in the biological context is a key technology, comprehensive knowledge of the physicochemical parameters under physiological conditions is of fundamental importance.

Nanoparticle characterization is a rich and complex discipline. In these exciting times for nanoscience, measurement and standardization often lag behind the rapid development of new materials and their applications. However, the demands on reproducibility and quality control increase steadily as new materials leave the discovery stage, and we expect that this pull will also drive innovations in the important field of nanoparticle-measurement science and technology.

Acknowledgements

All authors would like to acknowledge their families who have supported them throughout the writing process.

Conflict of Interest

The authors declare no conflict of interest.

Keywords

nanoparticle characterization, nanoparticles, porosity, shape, size, surface charge

Received: March 10, 2019
Revised: April 19, 2019
Published online:

[1] *Recommendation on the Definition of Nanomaterial*, European Commission, Brussels, Belgium **2011**, https://eur-lex.europa.eu/legal-content/EN/TXT/?uri=CELEX:32011H0696 (accessed: May 2019).
[2] D. V. Talapin, E. V. Shevchenko, *Chem. Rev.* **2016**, *116*, 10343.
[3] R. Kodama, *J. Magn. Magn. Mater.* **1999**, *200*, 359.
[4] H. Kim, R. P. Carney, J. Reguera, Q. K. Ong, X. Liu, F. Stellacci, *Adv. Mater.* **2012**, *24*, 3857.
[5] A. Cirri, A. Silakov, B. J. Lear, *Angew. Chem., Int. Ed.* **2015**, *54*, 11750.
[6] M. Reza Nejadnik, W. Jiskoot, *J. Pharm. Sci.* **2015**, *104*, 698.
[7] C. Gong, M. R. S. Dias, G. C. Wessler, J. A. Taillon, L. G. Salamanca-Riba, M. S. Leite, *Adv. Opt. Mater.* **2017**, *5*, 1600568.
[8] S. L. Lai, J. Y. Guo, V. Petrova, G. Ramanath, L. H. Allen, *Phys. Rev. Lett.* **1996**, *77*, 99.
[9] W. H. Qi, M. P. Wang, *J. Nanopart. Res.* **2005**, *7*, 51.
[10] S. Deshpande, S. Patil, S. V. Kuchibhatla, S. Seal, *Appl. Phys. Lett.* **2005**, *87*, 133113.
[11] M. Stratakis, H. Garcia, *Chem. Rev.* **2012**, *112*, 4469.
[12] F. Wang, H. Yu, S. Jeong, J. M. Pietryga, J. A. Hollingsworth, P. C. Gibbons, W. E. Buhro, *ACS Nano* **2008**, *2*, 1903.
[13] D. Segets, J. M. Lucas, R. N. Klupp Taylor, M. Scheele, H. Zheng, A. P. Alivisatos, W. Peukert, *ACS Nano* **2012**, *6*, 9021.
[14] W. Lin, *Chem. Rev.* **2015**, *115*, 10407.
[15] S. Kunjachan, J. Ehling, G. Storm, F. Kiessling, T. Lammers, *Chem. Rev.* **2015**, *115*, 10907.

 © 2019 WILEY-VCH Verlag GmbH & Co. KGaA, Weinheim

[16] A. B. Chinen, C. M. Guan, J. R. Ferrer, S. N. Barnaby, T. J. Merkel, C. A. Mirkin, *Chem. Rev.* **2015**, *115*, 10530.
[17] B. Pelaz, C. Alexiou, R. A. Alvarez-Puebla, F. Alves, A. M. Andrews, S. Ashraf, L. P. Balogh, L. Ballerini, A. Bestetti, C. Brendel, S. Bosi, M. Carril, W. C. W. Chan, C. Chen, X. Chen, X. Chen, Z. Cheng, D. Cui, J. Du, C. Dullin, A. Escudero, N. Feliu, M. Gao, M. George, Y. Gogotsi, A. Grünweller, Z. Gu, N. J. Halas, N. Hampp, R. K. Hartmann, M. C. Hersam, P. Hunziker, J. Jian, X. Jiang, P. Jungebluth, P. Kadhiresan, K. Kataoka, A. Khademhosseini, J. Kopeček, N. A. Kotov, H. F. Krug, D. S. Lee, C.-M. Lehr, K. W. Leong, X.-J. Liang, M. Ling Lim, L. M. Liz-Marzán, X. Ma, P. Macchiarini, H. Meng, H. Möhwald, P. Mulvaney, A. E. Nel, S. Nie, P. Nordlander, T. Okano, J. Oliveira, T. H. Park, R. M. Penner, M. Prato, V. Puntes, V. M. Rotello, A. Samarakoon, R. E. Schaak, Y. Shen, S. Sjöqvist, A. G. Skirtach, M. G. Soliman, M. M. Stevens, H.-W. Sung, B. Z. Tang, R. Tietze, B. N. Udugama, J. S. VanEpps, T. Weil, P. S. Weiss, I. Willner, Y. Wu, L. Yang, Z. Yue, Q. Zhang, Q. Zhang, X.-E. Zhang, Y. Zhao, X. Zhou, W. J. Parak, *ACS Nano* **2017**, *11*, 2313.
[18] R. Freund, U. Lächelt, T. Gruber, B. Rühle, S. Wuttke, *ACS Nano* **2018**, *12*, 2094.
[19] S. Wuttke, M. Lismont, A. Escudero, B. Rungtaweevoranit, W. J. Parak, *Biomaterials* **2017**, *123*, 172.
[20] D. Rosenblum, N. Joshi, W. Tao, J. M. Karp, D. Peer, *Nat. Commun.* **2018**, *9*, 1410.
[21] M. Peller, K. Böll, A. Zimpel, S. Wuttke, *Inorg. Chem. Front.* **2018**, *5*, 1760.
[22] F. Li, J. Lu, X. Kong, T. Hyeon, D. Ling, *Adv. Mater.* **2017**, *29*, 1605897.
[23] H. Goesmann, C. Feldmann, *Angew. Chem., Int. Ed.* **2010**, *49*, 1362.
[24] W. J. Stark, P. R. Stoessel, W. Wohlleben, A. Hafner, *Chem. Soc. Rev.* **2015**, *44*, 5793.
[25] M. Faria, M. Björnmalm, K. J. Thurecht, S. J. Kent, R. G. Parton, M. Kavallaris, A. P. R. Johnston, J. J. Gooding, S. R. Corrie, B. J. Boyd, P. Thordarson, A. K. Whittaker, M. M. Stevens, C. A. Prestidge, C. J. H. Porter, W. J. Parak, T. P. Davis, E. J. Crampin, F. Caruso, *Nat. Nanotechnol.* **2018**, *13*, 777.
[26] P. Hirschle, T. Preiß, F. Auras, A. Pick, J. Völkner, D. Valdepérez, G. Witte, W. J. Parak, J. O. Rädler, S. Wuttke, *CrystEngComm* **2016**, *18*, 4359.
[27] C. Y. Tay, M. I. Setyawati, J. Xie, W. J. Parak, D. T. Leong, *Adv. Funct. Mater.* **2014**, *24*, 5936.
[28] B. Demeler, T.-L. Nguyen, G. E. Gorbet, V. Schirf, E. H. Brookes, P. Mulvaney, A. O. El-Ballouli, J. Pan, O. M. Bakr, A. K. Demeler, B. I. Hernandez Uribe, N. Bhattarai, R. L. Whetten, *Anal. Chem.* **2014**, *86*, 7688.
[29] P. J. Wyatt, *Anal. Chem.* **2014**, *86*, 7171.
[30] E. J. Cho, H. Holback, K. C. Liu, S. A. Abouelmagd, J. Park, Y. Yeo, *Mol. Pharmaceutics* **2013**, *10*, 2093.
[31] Q. Ong, Z. Luo, F. Stellacci, *Acc. Chem. Res.* **2017**, *50*, 1911.
[32] Y. Ma, in *Toxicology of Nanomaterials*, Wiley-VCH Verlag GmbH & Co. KGaA (Eds: Y. Zhao, Z. Zhang, W. Feng), Weinheim, Germany **2016**, pp. 1–21.
[33] C. Jiang, Y. Cao, G. Xiao, R. Zhu, Y. Lu, *RSC Adv.* **2017**, *7*, 7531.
[34] D. Lee, M. F. Rubner, R. E. Cohen, *Nano Lett.* **2006**, *6*, 2305.
[35] S. Kumar, R. Rani, N. Dilbaghi, K. Tankeshwar, K.-H. Kim, *Chem. Soc. Rev.* **2017**, *46*, 158.
[36] S. Zhang, J. Li, G. Lykotrafitis, G. Bao, S. Suresh, *Adv. Mater.* **2009**, *21*, 419.
[37] H. H. Liu, S. Surawanvijit, R. Rallo, G. Orkoulas, Y. Cohen, *Environ. Sci. Technol.* **2011**, *45*, 9284.
[38] S. G. Elci, Y. Jiang, B. Yan, S. T. Kim, K. Saha, D. F. Moyano, G. Yesilbag Tonga, L. C. Jackson, V. M. Rotello, R. W. Vachet, *ACS Nano* **2016**, *10*, 5536.
[39] E. Blanco, H. Shen, M. Ferrari, *Nat. Biotechnol.* **2015**, *33*, 941.
[40] P. Horcajada, T. Chalati, C. Serre, B. Gillet, C. Sebrie, T. Baati, J. F. Eubank, D. Heurtaux, P. Clayette, C. Kreuz, J.-S. Chang, Y. K. Hwang, V. Marsaud, P.-N. Bories, L. Cynober, S. Gil, G. Férey, P. Couvreur, R. Gref, *Nat. Mater.* **2010**, *9*, 172.
[41] S. Wuttke, S. Braig, T. Preiß, A. Zimpel, J. Sicklinger, C. Bellomo, J. O. Rädler, A. M. Vollmar, T. Bein, *Chem. Commun.* **2015**, *51*, 15752.
[42] X. Liu, F. Zhang, X. Jing, M. Pan, P. Liu, W. Li, B. Zhu, J. Li, H. Chen, L. Wang, J. Lin, Y. Liu, D. Zhao, H. Yan, C. Fan, *Nature* **2018**, *559*, 593.
[43] B. Rühle, P. Saint-Cricq, J. I. Zink, *ChemPhysChem* **2016**, *17*, 1769.
[44] D. Tarn, C. E. Ashley, M. Xue, E. C. Carnes, J. I. Zink, C. J. Brinker, *Acc. Chem. Res.* **2013**, *46*, 792.
[45] R. A. Sperling, T. Liedl, S. Duhr, S. Kudera, M. Zanella, C.-A. J. Lin, W. H. Chang, D. Braun, W. J. Parak, *J. Phys. Chem. C* **2007**, *111*, 11552.
[46] ISO 13320:2009(en), Particle Size Analysis—Laser Diffraction Methods, https://www.iso.org/obp/ui/#iso:std:iso:13320:ed-1:v2:en (accessed: November 2018).
[47] N. Li, P. Zhao, D. Astruc, *Angew. Chem., Int. Ed.* **2014**, *53*, 1756.
[48] L. Talamini, M. B. Violatto, Q. Cai, M. P. Monopoli, K. Kantner, Ž. Krpetić, A. Perez-Potti, J. Cookman, D. Garry, C. P. Silveira, L. Boselli, B. Pelaz, T. Serchi, S. Cambier, A. C. Gutleb, N. Feliu, Y. Yan, M. Salmona, W. J. Parak, K. A. Dawson, P. Bigini, *ACS Nano* **2017**, *11*, 5519.
[49] A. Banerjee, J. Qi, R. Gogoi, J. Wong, S. Mitragotri, *J. Controlled Release* **2016**, *238*, 176.
[50] C. Forestiere, G. Miano, S. V. Boriskina, L. Dal Negro, *Opt. Express* **2009**, *17*, 9648.
[51] C. J. Orendorff, T. K. Sau, C. J. Murphy, *Small* **2006**, *2*, 636.
[52] J. Park, H. Elmlund, P. Ercius, J. M. Yuk, D. T. Limmer, Q. Chen, K. Kim, S. H. Han, D. A. Weitz, A. Zettl, A. P. Alivisatos, *Science* **2015**, *349*, 290.
[53] P. Ercius, O. Alaidi, M. J. Rames, G. Ren, *Adv. Mater.* **2015**, *27*, 5638.
[54] B. Chu, T. Liu, *J. Nanopart. Res.* **2000**, *2*, 29.
[55] Y. Ju-Nam, J. R. Lead, *Sci. Total Environ.* **2008**, *400*, 396.
[56] V. S. Kulkarni, *Handbook of Non-Invasive Drug Delivery Systems: Science and Technology*, William Andrew, Oxford **2009**.
[57] A. D. McNaught, A. Wilkinson, *IUPAC Compendium of Chemical Terminology*, 2nd ed., Blackwell Scientific Publications, Oxford **1997**, https://doi.org/10.1351/goldbook.P04704.
[58] U. Sakulkhu, M. Mahmoudi, L. Maurizi, G. Coullerez, M. Hofmann-Amtenbrink, M. Vries, M. Motazacker, F. Rezaee, H. Hofmann, *Biomater. Sci.* **2015**, *3*, 265.
[59] D. H. Jo, J. H. Kim, T. G. Lee, J. H. Kim, *Nanomedicine* **2015**, *11*, 1603.
[60] A. Baeza, D. Ruiz-Molina, M. Vallet-Regí, *Expert Opin. Drug Delivery* **2017**, *14*, 783.
[61] J. Liu, C. Wu, D. Xiao, P. Kopold, L. Gu, P. A. van Aken, J. Maier, Y. Yu, *Small* **2016**, *12*, 2354.
[62] Y. Min, J. M. Caster, M. J. Eblan, A. Z. Wang, *Chem. Rev.* **2015**, *115*, 11147.
[63] H. Cabral, K. Miyata, K. Osada, K. Kataoka, *Chem. Rev.* **2018**, *118*, 6844.
[64] J. Shi, P. W. Kantoff, R. Wooster, O. C. Farokhzad, *Nat. Rev. Cancer* **2017**, *17*, 20.
[65] A. Z. Wang, R. Langer, O. C. Farokhzad, *Annu. Rev. Med.* **2012**, *63*, 185.
[66] N. Lee, D. Yoo, D. Ling, M. H. Cho, T. Hyeon, J. Cheon, *Chem. Rev.* **2015**, *115*, 10637.
[67] Z. Li, D. L. Clemens, B.-Y. Lee, B. J. Dillon, M. A. Horwitz, J. I. Zink, *ACS Nano* **2015**, *9*, 10778.

© 2019 WILEY-VCH Verlag GmbH & Co. KGaA, Weinheim

[68] Z. Li, J. C. Barnes, A. Bosoy, J. F. Stoddart, J. I. Zink, *Chem. Soc. Rev.* **2012**, *41*, 2590.
[69] D. B. Williams, C. B. Carter, *Transmission Electron Microscopy*, Springer US, Boston, MA **2009**.
[70] A. Surrey, D. Pohl, L. Schultz, B. Rellinghaus, *Nano Lett.* **2012**, *12*, 6071.
[71] M. A. O'Keefe, Y. Shao-Horn, *Microsc. Microanal.* **2004**, *10*, 86.
[72] U. Dahmen, R. Erni, V. Radmilovic, C. Ksielowski, M.-D. Rossell, P. Denes, *Philos. Trans. R. Soc., A* **2009**, *367*, 3795.
[73] W. Zhou, H. F. Greer, *Eur. J. Inorg. Chem.* **2016**, *2016*, 941.
[74] I. Srnová-Šloufová, F. Lednický, A. Gemperle, J. Gemperlová, *Langmuir* **2000**, *16*, 9928.
[75] M. T. Reetz, M. Maase, T. Schilling, B. Tesche, *J. Phys. Chem. B* **2000**, *104*, 8779.
[76] S. Mondini, A. M. Ferretti, A. Puglisi, A. Ponti, *Nanoscale* **2012**, *4*, 5356.
[77] C. R. Murthy, B. Gao, A. R. Tao, G. Arya, *Nanoscale* **2015**, *7*, 9793.
[78] E. V. Orlova, H. R. Saibil, *Chem. Rev.* **2011**, *111*, 7710.
[79] W. Anderson, D. Kozak, V. A. Coleman, Å. K. Jämting, M. Trau, *J. Colloid Interface Sci.* **2013**, *405*, 322.
[80] E. Nakamura, N. A. J. M. Sommerdijk, H. Zheng, *Acc. Chem. Res.* **2017**, *50*, 1795.
[81] S. T. Skowron, T. W. Chamberlain, J. Biskupek, U. Kaiser, E. Besley, A. N. Khlobystov, *Acc. Chem. Res.* **2017**, *50*, 1797.
[82] J. P. Patterson, Y. Xu, M.-A. Moradi, N. A. J. M. Sommerdijk, H. Friedrich, *Acc. Chem. Res.* **2017**, *50*, 1495.
[83] J. Goldstein, D. E. Newbury, J. R. Michael, N. W. M. Ritchie, J. H. J. Scott, D. C. Joy, *Scanning Electron Microscopy and X-Ray Microanalysis*, Springer-Verlag, New York **2018**.
[84] S. Rades, V.-D. Hodoroaba, T. Salge, T. Wirth, M. P. Lobera, R. H. Labrador, K. Natte, T. Behnke, T. Gross, W. E. S. Unger, *RSC Adv.* **2014**, *4*, 49577.
[85] E. Buhr, N. Senftleben, T. Klein, D. Bergmann, D. Gnieser, C. G. Frase, H. Bosse, *Meas. Sci. Technol.* **2009**, *20*, 084025.
[86] S. Mourdikoudis, R. M. Pallares, N. T. K. Thanh, *Nanoscale* **2018**, *10*, 12871.
[87] D. J. Stokes, *Microsc. Microanal.* September **2012**, 67.
[88] P. Luo, I. Morrison, A. Dudkiewicz, K. Tiede, E. Boyes, P. O'Toole, S. Park, A. B. Boxall, *J. Microsc.* **2013**, *250*, 32.
[89] Y. Seo, W. Jhe, *Rep. Prog. Phys.* **2008**, *71*, 016101.
[90] H.-J. Butt, B. Cappella, M. Kappl, *Surf. Sci. Rep.* **2005**, *59*, 1.
[91] S. Morita, R. Wiesendanger, E. Meyer, *Noncontact Atomic Force Microscopy*, Springer, Berlin **2002**.
[92] M. Lanza, *Conductive Atomic Force Microscopy: Applications in Nanomaterials*, Wiley-VCH Verlag GmbH & Co. KGaA, Weinheim, Germany **2017**.
[93] F. J. Giessibl, *Rev. Mod. Phys.* **2003**, *75*, 949.
[94] U. Holzwarth, N. Gibson, *Nat. Nanotechnol.* **2011**, *6*, 534.
[95] P. Scherrer, *Nachr. Akad. Wiss. Goettingen, Math.-Phys. Kl.* **1918**, *1918*, 98.
[96] H. Klug, L. Alexander, *X-Ray Diffraction Procedures: For Polycrystalline and Amorphous Materials*, 2nd ed., John Wiley & Sons, New York **1974**.
[97] S. Britto, S. Joseph, P. Vishnu Kamath, *J. Chem. Sci.* **2010**, *122*, 751.
[98] P. Muhammed Shafi, A. Chandra Bose, *AIP Adv.* **2015**, *5*, 057137.
[99] A. V. Vorontsov, S. V. Tsybulya, *Ind. Eng. Chem. Res.* **2018**, *57*, 2526.
[100] I. Robinson, *J. Phys. Soc. Jpn.* **2013**, *82*, 021012.
[101] A. Cervellino, R. Frison, N. Masciocchi, A. Guagliardi, in *X-Ray and Neutron Techniques for Nanomaterials Characterization* (Ed: C. Kumar), Springer, Berlin **2016**, pp. 545–608.
[102] T. Li, A. J. Senesi, B. Lee, *Chem. Rev.* **2016**, *116*, 11128.
[103] A. G. Kikhney, D. I. Svergun, *FEBS Lett.* **2015**, *589*, 2570.
[104] H. Takeno, in *X-Ray and Neutron Techniques for Nanomaterials Characterization* (Ed: C. Kumar), Springer, Berlin **2016**, pp. 717–760.
[105] J. M. Costa-Fernández, M. Menéndez-Miranda, D. Bouzas-Ramos, J. R. Encinar, A. Sanz-Medel, *TrAC Trends Anal. Chem.* **2016**, *84*, 139.
[106] A. R. M. Bustos, J. R. Encinar, A. Sanz-Medel, *Anal. Bioanal. Chem.* **2013**, *405*, 5637.
[107] E. A. Kapellios, S. A. Pergantis, *J. Anal. At. Spectrom.* **2012**, *27*, 21.
[108] S. Gschwind, L. Flamigni, J. Koch, O. Borovinskaya, S. Groh, K. Niemax, D. Günther, *J. Anal. At. Spectrom.* **2011**, *26*, 1166.
[109] A. Kasuya, R. Sivamohan, Y. A. Barnakov, I. M. Dmitruk, T. Nirasawa, V. R. Romanyuk, V. Kumar, S. V. Mamykin, K. Tohji, B. Jeyadevan, K. Shinoda, T. Kudo, O. Terasaki, Z. Liu, R. V. Belosludov, V. Sundararajan, Y. Kawazoe, *Nat. Mater.* **2004**, *3*, 99.
[110] S. Jeon, D. R. Oberreit, G. Van Schooneveld, C. J. Hogan, *Analyst* **2016**, *141*, 1363.
[111] S. Elzey, D.-H. Tsai, L. L. Yu, M. R. Winchester, M. E. Kelley, V. A. Hackley, *Anal. Bioanal. Chem.* **2013**, *405*, 2279.
[112] C. Degueldre, P.-Y. Favarger, *Colloids Surf. A* **2003**, *217*, 137.
[113] J. K. Navin, M. E. Grass, G. A. Somorjai, A. L. Marsh, *Anal. Chem.* **2009**, *81*, 6295.
[114] S. Nicolardi, Y. E. M. van der Burgt, J. D. C. Codée, M. Wuhrer, C. H. Hokke, F. Chiodo, *ACS Nano* **2017**, *11*, 8257.
[115] H. Hinterwirth, S. Kappel, T. Waitz, T. Prohaska, W. Lindner, M. Lämmerhofer, *ACS Nano* **2013**, *7*, 1129.
[116] N. Fernández-Iglesias, J. Bettmer, *Nanoscale* **2015**, *7*, 14324.
[117] F. Chen, G. Wang, J. I. Griffin, B. Brenneman, N. K. Banda, V. M. Holers, D. S. Backos, L. Wu, S. M. Moghimi, D. Simberg, *Nat. Nanotechnol.* **2017**, *12*, 387.
[118] M. Magro, M. Zaccarin, G. Miotto, L. Da Dalt, D. Baratella, P. Fariselli, G. Gabai, F. Vianello, *Anal. Bioanal. Chem.* **2018**, *410*, 2949.
[119] S. Chen, C. Xiong, H. Liu, Q. Wan, J. Hou, Q. He, A. Badu-Tawiah, Z. Nie, *Nat. Nanotechnol.* **2015**, *10*, 176.
[120] D. P. Bishop, M. Grossgarten, D. Dietrich, A. Vennemann, N. Cole, M. Sperling, M. Wiemann, P. A. Doble, U. Karst, *Anal. Methods* **2018**, *10*, 836.
[121] K. S. W. Sing, *Colloids Surf.* **1989**, *38*, 113.
[122] K. A. Cychosz, M. Thommes, *Engineering* **2018**, *4*, 559.
[123] M. Thommes, K. Kaneko, A. V. Neimark, J. P. Olivier, F. Rodriguez-Reinoso, J. Rouquerol, K. S. W. Sing, *Pure Appl. Chem.* **2015**, *87*, 1051.
[124] A. J. Lecloux, *J. Nanopart. Res.* **2015**, *17*, 447.
[125] A. J. Lecloux, R. Atluri, Y. V. Kolen'ko, F. L. Deepak, *Nanoscale* **2017**, *9*, 14952.
[126] E. A. Van Doren, P.-J. R. De Temmerman, M. Francisco, J. Mast, *J. Nanobiotechnol.* **2011**, *9*, 17.
[127] W. Wohlleben, J. Mielke, A. Bianchin, A. Ghanem, H. Freiberger, H. Rauscher, M. Gemeinert, V.-D. Hodoroaba, *J. Nanopart. Res.* **2017**, *19*, 61.
[128] Scientific Committee on Emerging and Newly Identified Health Risks, *Scientific Basis for the Definition of the Term "Nanomaterial"*, European Commission, Brussels, Belgium **2010**.
[129] W. G. Kreyling, M. Semmler-Behnke, Q. Chaudhry, *Nano Today* **2010**, *5*, 165.
[130] R. Pecora, *J. Nanopart. Res.* **2000**, *2*, 123.
[131] D. E. Koppel, *J. Chem. Phys.* **1972**, *57*, 4814.
[132] I. D. Morrison, E. F. Grabowski, C. A. Herb, *Langmuir* **1985**, *1*, 496.
[133] A. Scotti, W. Liu, J. S. Hyatt, E. S. Herman, H. S. Choi, J. W. Kim, L. A. Lyon, U. Gasser, A. Fernandez-Nieves, *J. Chem. Phys.* **2015**, *142*, 234905.
[134] J. Stetefeld, S. A. McKenna, T. R. Patel, *Biophys. Rev.* **2016**, *8*, 409.
[135] F. Varenne, A. Makky, M. Gaucher-Delmas, F. Violleau, C. Vauthier, *Pharm. Res.* **2016**, *33*, 1220.
[136] S. K. Brar, M. Verma, *TrAC Trends Anal. Chem.* **2011**, *30*, 4.

© 2019 WILEY-VCH Verlag GmbH & Co. KGaA, Weinheim

[137] H. Qian, M. P. Sheetz, E. L. Elson, *Biophys. J.* **1991**, *60*, 910.
[138] V. Filipe, A. Hawe, W. Jiskoot, *Pharm. Res.* **2010**, *27*, 796.
[139] S. Bhattacharjee, *J. Controlled Release* **2016**, *235*, 337.
[140] B. R. Ware, W. H. Flygare, *Chem. Phys. Lett.* **1971**, *12*, 81.
[141] R. Xu, *Particuology* **2008**, *6*, 112.
[142] R. P. Carney, J. Y. Kim, H. Qian, R. Jin, H. Mehenni, F. Stellacci, O. M. Bakr, *Nat. Commun.* **2011**, *2*, 335.
[143] P. Schuck, H. Zhao, C. Brautigam, R. Ghirlando, *Basic Principles of Analytical Ultracentrifugation*, CRC Press, Boca raton, FL **2015**.
[144] Ž. Krpetić, A. M. Davidson, M. Volk, R. Lévy, M. Brust, D. L. Cooper, *ACS Nano* **2013**, *7*, 8881.
[145] A. Bekdemir, F. Stellacci, *Nat. Commun.* **2016**, *7*, 13121.
[146] J. Walter, K. Löhr, E. Karabudak, W. Reis, J. Mikhael, W. Peukert, W. Wohlleben, H. Cölfen, *ACS Nano* **2014**, *8*, 8871.
[147] L. Pitkänen, A. M. Striegel, *TrAC Trends Anal. Chem.* **2016**, *80*, 311.
[148] A. Podgornik, S. Yamamoto, M. Peterka, N. L. Krajnc, *J. Chromatogr. B* **2013**, *927*, 80.
[149] G.-T. Wei, F.-K. Liu, C. R. C. Wang, *Anal. Chem.* **1999**, *71*, 2085.
[150] K. M. Krueger, A. M. Al-Somali, J. C. Falkner, V. L. Colvin, *Anal. Chem.* **2005**, *77*, 3511.
[151] Z. Aspanut, T. Yamada, L. W. Lim, T. Takeuchi, *Anal. Bioanal. Chem.* **2008**, *391*, 353.
[152] S. Süß, C. Metzger, C. Damm, D. Segets, W. Peukert, *Powder Technol.* **2018**, *339*, 264.
[153] J. D. Robertson, L. Rizzello, M. Avila-Olias, J. Gaitzsch, C. Contini, M. S. Magoń, S. A. Renshaw, G. Battaglia, *Sci. Rep.* **2016**, *6*, 27494.
[154] J. C. Giddings, *Science* **1993**, *260*, 1456.
[155] G. Moreno-Martin, J. Sanz-Landaluze, Y. Madrid, in *Encyclopedia of Analytical Chemistry* (Ed: R. A. Meyers), John Wiley & Sons, Ltd, Chichester, UK **2017**, pp. 1–24.
[156] S. K. R. Williams, J. R. Runyon, A. A. Ashames, *Anal. Chem.* **2011**, *83*, 634.
[157] K.-G. Wahlund, *J. Chromatogr. A* **2013**, *1287*, 97.
[158] K. Bacia, P. Schwille, *Methods* **2003**, *29*, 74.
[159] K. Bacia, S. A. Kim, P. Schwille, *Nat. Methods* **2006**, *3*, 83.
[160] N. Pal, S. D. Verma, M. K. Singh, S. Sen, *Anal. Chem.* **2011**, *83*, 7736.
[161] K. Starchev, J. Zhang, J. Buffle, *J. Colloid Interface Sci.* **1998**, *203*, 189.
[162] A. Zimpel, N. Al Danaf, B. Steinborn, J. Kuhn, M. Hoehn, T. Bauer, P. Hirschle, W. Schrimpf, H. Engelke, E. Wagner, M. Barz, D. C. Lamb, U. Lächelt, S. Wuttke, *ACS Nano* **2019**, *13*, 3884.
[163] G. R. Willmott, *Anal. Chem.* **2018**, *90*, 2987.
[164] A. K. Pal, I. Aalaei, S. Gadde, P. Gaines, D. Schmidt, P. Demokritou, D. Bello, *ACS Nano* **2014**, *8*, 9003.
[165] E. Weatherall, G. R. Willmott, *Analyst* **2015**, *140*, 3318.
[166] M. Platt, G. R. Willmott, G. U. Lee, *Small* **2012**, *8*, 2436.
[167] M. J. Williamson, R. M. Tromp, P. M. Vereecken, R. Hull, F. M. Ross, *Nat. Mater.* **2003**, *2*, 532.
[168] S. F. Tan, S. W. Chee, G. Lin, U. Mirsaidov, *Acc. Chem. Res.* **2017**, *50*, 1303.
[169] H. Zheng, R. K. Smith, Y.-w. Jun, C. Kisielowski, U. Dahmen, A. P. Alivisatos, *Science* **2009**, *324*, 1309.
[170] N. de Jonge, L. Houben, R. E. Dunin-Borkowski, F. M. Ross, *Nat. Rev. Mater.* **2019**, *4*, 61.
[171] L. R. Parent, E. Bakalis, M. Proetto, Y. Li, C. Park, F. Zerbetto, N. C. Gianneschi, *Acc. Chem. Res.* **2018**, *51*, 3.
[172] N. D. Loh, S. Sen, M. Bosman, S. F. Tan, J. Zhong, C. A. Nijhuis, P. Král, P. Matsudaira, U. Mirsaidov, *Nat. Chem.* **2017**, *9*, 77.
[173] U. Anand, J. Lu, D. Loh, Z. Aabdin, U. Mirsaidov, *Nano Lett.* **2016**, *16*, 786.
[174] G. Lin, S. W. Chee, S. Raj, P. Král, U. Mirsaidov, *ACS Nano* **2016**, *10*, 7443.
[175] Q. Chen, H. Cho, K. Manthiram, M. Yoshida, X. Ye, A. P. Alivisatos, *ACS Cent. Sci.* **2015**, *1*, 33.
[176] S. F. Tan, U. Anand, U. Mirsaidov, *ACS Nano* **2017**, *11*, 1633.
[177] E. Nakamura, *Acc. Chem. Res.* **2017**, *50*, 1281.
[178] R. M. Gorgoll, E. Yücelen, A. Kumamoto, N. Shibata, K. Harano, E. Nakamura, *J. Am. Chem. Soc.* **2015**, *137*, 3474.
[179] M. Koshino, T. Tanaka, N. Solin, K. Suenaga, H. Isobe, E. Nakamura, *Science* **2007**, *316*, 853.
[180] R. Fernandez-Leiro, S. H. W. Scheres, *Nature* **2016**, *537*, 339.
[181] P. L. Stewart, *Wiley Interdiscip. Rev.: Nanomed. Nanobiotechnol.* **2017**, *9*, e1417.
[182] T. Gonen, Y. Cheng, P. Sliz, Y. Hiroaki, Y. Fujiyoshi, S. C. Harrison, T. Walz, *Nature* **2005**, *438*, 633.
[183] Y. Cheng, *Science* **2018**, *361*, 876.
[184] A. Wittemann, M. Drechsler, Y. Talmon, M. Ballauff, *J. Am. Chem. Soc.* **2005**, *127*, 9688.
[185] J. Radon, *Math. Phys. Kl.* **1917**, *69*, 262.
[186] Z. Saghi, P. A. Midgley, *Annu. Rev. Mater. Res.* **2012**, *42*, 59.
[187] J. Miao, P. Ercius, S. J. L. Billinge, *Science* **2016**, *353*, aaf2157.
[188] C. Bonnaud, C. A. Monnier, D. Demurtas, C. Jud, D. Vanhecke, X. Montet, R. Hovius, M. Lattuada, B. Rothen-Rutishauser, A. Petri-Fink, *ACS Nano* **2014**, *8*, 3451.
[189] D. Armitage, F. P. Price, *Chem. Phys. Lett.* **1976**, *44*, 305.
[190] C. L. Jackson, G. B. McKenna, *J. Chem. Phys.* **1990**, *93*, 9002.
[191] G. Fagerlund, *Mater. Constr.* **1973**, *6*, 215.
[192] M. Brun, A. Lallemand, J.-F. Quinson, C. Eyraud, *Thermochim. Acta* **1977**, *21*, 59.
[193] J. H. Strange, M. Rahman, E. G. Smith, *Phys. Rev. Lett.* **1993**, *71*, 3589.
[194] J. Mitchell, J. B. W. Webber, J. H. Strange, *Phys. Rep.* **2008**, *461*, 1.
[195] J. Park, A. Byun, D.-H. Kim, S. S. Shin, J.-H. Kim, J. W. Kim, *J. Colloid Interface Sci.* **2014**, *426*, 162.
[196] N. Rescignano, M. Amelia, A. Credi, J. M. Kenny, I. Armentano, *Eur. Polym. J.* **2012**, *48*, 1152.
[197] N. Gopinathan, B. Yang, J. P. Lowe, K. J. Edler, S. P. Rigby, *Int. J. Pharm.* **2014**, *469*, 146.
[198] S. J. Sahl, S. W. Hell, S. Jakobs, *Nat. Rev. Mol. Cell Biol.* **2017**, *18*, 685.
[199] D. Wöll, C. Flors, *Small Methods* **2017**, *1*, 1700191.
[200] J. J. Richardson, H. Ejima, S. L. Lörcher, K. Liang, P. Senn, J. Cui, F. Caruso, *Angew. Chem.* **2013**, *125*, 6583.
[201] A. P. H. Gelissen, A. Oppermann, T. Caumanns, P. Hebbeker, S. K. Turnhoff, R. Tiwari, S. Eisold, U. Simon, Y. Lu, J. Mayer, W. Richtering, A. Walther, D. Wöll, *Nano Lett.* **2016**, *16*, 7295.
[202] G. M. Conley, S. Nöjd, M. Braibanti, P. Schurtenberger, F. Scheffold, *Colloids Surf. A* **2016**, *499*, 18.
[203] A. M. Clemments, P. Botella, C. C. Landry, *J. Am. Chem. Soc.* **2017**, *139*, 3978.
[204] B. Rühle, M. Davies, T. Bein, C. Bräuchle, *Z. Naturforsch., B: J. Chem. Sci.* **2013**, *68*, 423.
[205] T. Lebold, J. Michaelis, C. Bräuchle, *Phys. Chem. Chem. Phys.* **2011**, *13*, 5017.
[206] A. Zürner, J. Kirstein, M. Döblinger, C. Bräuchle, T. Bein, *Nature* **2007**, *450*, 705.
[207] B. Rühle, M. Davies, T. Lebold, C. Bräuchle, T. Bein, *ACS Nano* **2012**, *6*, 1948.
[208] M. Davies, B. Rühle, C. Li, K. Müllen, T. Bein, C. Bräuchle, *J. Phys. Chem. C* **2014**, *118*, 24013.
[209] F. Feil, V. Cauda, T. Bein, C. Bräuchle, *Nano Lett.* **2012**, *12*, 1354.
[210] T. Lebold, L. A. Mühlstein, J. Blechinger, M. Riederer, H. Amenitsch, R. Köhn, K. Peneva, K. Müllen, J. Michaelis, C. Bräuchle, T. Bein, *Chem. — Eur. J.* **2009**, *15*, 1661.
[211] T. Lebold, A. Schlossbauer, K. Schneider, L. Schermelleh, H. Leonhardt, T. Bein, C. Bräuchle, *Adv. Funct. Mater.* **2012**, *22*, 106.
[212] E. Sage, M. Sansa, S. Fostner, M. Defoort, M. Gély, A. K. Naik, R. Morel, L. Duraffourg, M. L. Roukes, T. Alava, G. Jourdan, E. Colinet, C. Masselon, A. Brenac, S. Hentz, *Nat. Commun.* **2018**, *9*, 3283.

© 2019 WILEY-VCH Verlag GmbH & Co. KGaA, Weinheim

[213] J. E. Sader, M. S. Hanay, A. P. Neumann, M. L. Roukes, *Nano Lett.* **2018**, *18*, 1608.
[214] T. P. Burg, M. Godin, S. M. Knudsen, W. Shen, G. Carlson, J. S. Foster, K. Babcock, S. R. Manalis, *Nature* **2007**, *446*, 1066.
[215] S. Olcum, N. Cermak, S. C. Wasserman, K. S. Christine, H. Atsumi, K. R. Payer, W. Shen, J. Lee, A. M. Belcher, S. N. Bhatia, S. R. Manalis, *Proc. Natl. Acad. Sci. USA* **2014**, *111*, 1310.
[216] M. M. Modena, Y. Wang, D. Riedel, T. P. Burg, *Lab Chip* **2014**, *14*, 342.
[217] M. M. Modena, P. Hirschle, S. Wuttke, T. P. Burg, *Small* **2018**, *14*, 1800826.
[218] A. Cox, P. Andreozzi, R. Dal Magro, F. Fiordaliso, A. Corbelli, L. Talamini, C. Chinello, F. Raimondo, F. Magni, M. Tringali, S. Krol, P. Jacob Silva, F. Stellacci, M. Masserini, F. Re, *ACS Nano* **2018**, *12*, 7292.

© 2019 WILEY-VCH Verlag GmbH & Co. KGaA, Weinheim